NUREG/CR-4667 Vol. II
ANL-86-37

Materials and Components
Technology Division
Materials and Components
Technology Division
Materials and Components
Technology Division

Environmentally Assisted Cracking in Light Water Reactors: Semiannual Report

October 1985–March 1986

by W. J. Shack, T. F. Kassner, P. S. Maiya,
J. Y. Park, and W. E. Ruther

Argonne National Laboratory, Argonne, Illinois 60439
operated by The University of Chicago
Prepared for the Office of Nuclear Regulatory Research
U. S. Nuclear Regulatory Commission under Interagency Agreement DOE 40-550-75

NUREG/CR-4667 Vol. II
ANL-86-37
Distribution Code: R5

NUREG/CR--4667-Vol.2

TI87 000853

ARGONNE NATIONAL LABORATORY
9700 South Cass Avenue
Argonne, Illinois 60439

ENVIRONMENTALLY ASSISTED CRACKING IN LIGHT WATER REACTORS: SEMIANNUAL REPORT

October 1985--March 1986

by

W. J. Shack, T. F. Kassner, P. S. Maiya,
J. Y. Park, and W. E. Ruther

Materials and Components Technology Division

Report Completed
July 1986

Previous Reports in this series

ANL-85-33	October 1983--September 1984
ANL-84-60 Vol. III	October--December 1984
ANL-85-75 Vol. I	January--March 1985
ANL-86-31	April--September 1985

Prepared for the Division of Engineering Technology
Office of Nuclear Regulatory Research
U. S. Nuclear Regulatory Commission
Washington, D. C. 20555
Under Interagency Agreement DOE 40-550-75

NRC FIN No. A2212

ENVIRONMENTALLY ASSISTED CRACKING IN LIGHT WATER REACTORS:
SEMIANNUAL REPORT

October 1985--March 1986

ABSTRACT

This progress report summarizes work performed by Argonne National Laboratory on environmentally assisted cracking in light water reactors during the six months from October 1985 to March 1986.

NRC Fin No.	FIN Title
A2212	Environmentally Assisted Cracking in Light-Water Reactors

TABLE OF CONTENTS

ENVIRONMENTALLY ASSISTED CRACKING IN LIGHT WATER REACTORS: SEMIANNUAL REPORT[a]

October 1985--March 1986

EXECUTIVE SUMMARY

Analyses have been performed on weldments treated by the mechanical stress improvement process (MSIP) developed by O'Donnell and Associates, Inc. The weldments were evaluated by dye penetrant, ultrasonic, and metallographic techniques, and measurements of residual stress were made. The residual stress measurements indicate that the axial stress on the inner surface in the heat-affected zone was strongly compressive (-30 to -50 ksi). Although analytical results suggest that the stresses directly under the MSIP tool will be tensile, the measured stresses were also compressive (-15 ksi). Shallow circumferential cracks were found in the fillet of the counterbore region on the inner surface of a 12-in.-diameter MSIP-treated weldment which was exposed to boiling $MgCl_2$. The cracks were transgranular and branched, which is indicative of chloride-induced stress corrosion cracking (SCC). Longitudinal cracks were detected on the inner surface of the pipe along the fusion line of a seam weld almost directly under the MSIP tool, and circumferential cracks were also found in the heat-affected zone of another weld that was not MSIP-treated. All of the observed cracking is attributed to chloride-induced SCC in regions of localized tensile stresses. A 28-in.-diameter weldment that has been treated by MSIP but not exposed to boiling $MgCl_2$ is being examined to resolve the issue of cracking in the previous weldment.

The SCC susceptibility of the base material and weldments of German TP 347 stainless steel (SS) is being investigated in constant-extension-rate-tensile CERT experiments in high-temperature water containing dissolved oxygen and sulfate as an impurity at low concentrations. The SCC susceptibility of TP 347 SS appears very similar to that of Type 316NG SS; i.e., the material is susceptible to transgranular SCC in impurity environments at low strain rates.

---

[a]NRC FIN No. A2212; NRC Contact: A. Taboada.

However, failure of the weldment specimens always occurred in the base metal, and there was no evidence of "knife-line attack" adjacent to the fusion zone.

Additional data have been analyzed in terms of the phenomenological model for SCC, which is based on a simplified elastic-plastic fracture mechanics analysis and a slip-dissolution mechanism of crack advance. The capability of the model to correlate crack growth results for Types 304 and 316 SS as well as the alternative materials (viz., Types 316NG, 316LN, and 347NG) has been demonstrated.

Fracture mechanics crack growth rate tests are being performed to determine the inherent stress corrosion crack growth resistance of the Type 308L weld metal used for weld overlay repairs. The crack growth rate in a Type 304 SS/ER 308L SS weld overlay specimen, fabricated from a 10-in.-diameter pipe with an overlay applied by standard nuclear industry practice, has been measured in simulated BWR-quality water under low-frequency cyclic-loading conditions at 289°C. The specimen was fabricated such that the crack propagates through the original sensitized pipe material into the ER 308L SS overlay. The results of the ongoing experiment indicate that the crack growth rate in the weld overlay is virtually the same as in underlying pipe material, although the test is still in progress and the results have not been verified metallographically.

Validation of the premise that SCC of sensitized Type 304 SS is controlled by the rate of cathodic reduction of dissolved oxygen and/or various oxyanions would provide a basis for understanding the potential effects of a large class of impurities on SCC. As part of the continuing program to explore this premise, several CERT experiments were performed in 289°C water containing 0.2 ppm oxygen and $Na_2B_4O_7$ at low concentrations. The addition of $Na_2B_4O_7$ to the feedwater provides an anion that is relatively innocuous from the standpoint of SCC and could adsorb on the oxide surface and conceivably compete for sites available for oxygen reduction. In contrast to previous results, in which $Na_2B_4O_7$ additions to low-oxygen water containing sulfate impurity markedly decreased SCC susceptibility of the steel, no benefit was derived from $Na_2B_4O_7$ additions to the oxygenated high-purity water.

ENVIRONMENTALLY ASSISTED CRACKING IN LIGHT-WATER REACTORS: SEMIANNUAL REPORT
October 1985--March 1986

Principal Investigators:
W. J. Shack, T. F. Kassner, P. S. Maiya,
J. Y. Park, and W. E. Ruther

The objective of this program is to develop an independent capability for prediction, detection, and control of intergranular stress corrosion cracking (IGSCC) in light-water reactor (LWR) systems. The program is primarily directed at IGSCC problems in existing plants, but also includes the development of recommendations for plants under construction and future plants. The scope includes the following: (1) evaluation of the influence of metallurgical variables, stress, and the environment on IGSCC susceptibility, including the influence of plant operations on these variables; and (2) examination of practical limits for these variables to effectively control IGSCC in LWR systems. The experimental work concentrates primarily on problems related to pipe cracking in BWR systems. However, ongoing research work on other environmentally assisted cracking problems involving pressure vessels, nozzles, and turbines will be monitored and assessed, and where unanswered technical questions are identified, experimental programs to obtain the necessary information will be developed to the extent that resources permit.

The effort during this reporting period is divided into three subtasks: (A) Effects of Long-Term Aging and Analysis of Reactor Components; (B) Evaluation of Nonenvironmental Corrective Actions; and (C) Evaluation of Environmental Corrective Actions. These subtasks reflect the major technical concerns associated with IGSCC in LWR systems: the role of materials susceptibility, the role of stress in crack initiation and propagation, and the role of environment. The program seeks to evaluate potential solutions to IGSCC problems in LWRs, both by direct experimentation (including full-scale pipe tests) and through the development of a better understanding of the various phenomena.

A. Effects of Long-Term Aging and Analysis of Reactor Components (J. Y. Park and W. J. Shack)

1. Introduction

Microstructural changes resulting from thermal exposure can have a profound influence on the susceptibility to intergranular corrosion. In conventional austenitic stainless steels, the most important microstructural change is sensitization, i.e., the depletion of chromium from the grain boundaries caused by the precipitation of grain boundary carbides. However, segregation of impurity elements such as phosphorus and sulfur can also occur during thermal exposure and affect susceptibility to stress corrosion. In this task, the effects of long-term aging on alternative materials such as Type 316NG and the German Type 347 stainless steels are being studied. The effects of remedy and repair procedures such as induction heating stress improvement (IHSI), mechanical stress improvement process (MSIP), and weld overlays on the subsequent behavior of sensitized Type 304 stainless steel during long-term aging are also being considered.

In addition, this task is also concerned with characterization of the other changes such as induced residual stresses and possible effects of the associated plastic strains produced in reactor components by remedy and repair procedures. Many of the studies must be carried out on mock-up weldments, but when possible, in-reactor components have been obtained and are being analyzed to assess the effectiveness of the remedial treatments and to verify the results of in-service inspections.

2. Technical Progress

a. Metallographic Studies of the Mechanical Stress Improvement Process (J. Y. Park)

Metallurgical sections were cut from the 12-in.-diameter weldment which was prepared by Vermont Yankee Nuclear Power Corp. and treated by the MSIP process developed by O'Donnell and Associates, Inc. (OAI). There are two welds in the test piece, as shown in Fig. 1. The upper weld received the MSIP treatment in accordance with OAI specifications. The MSIP

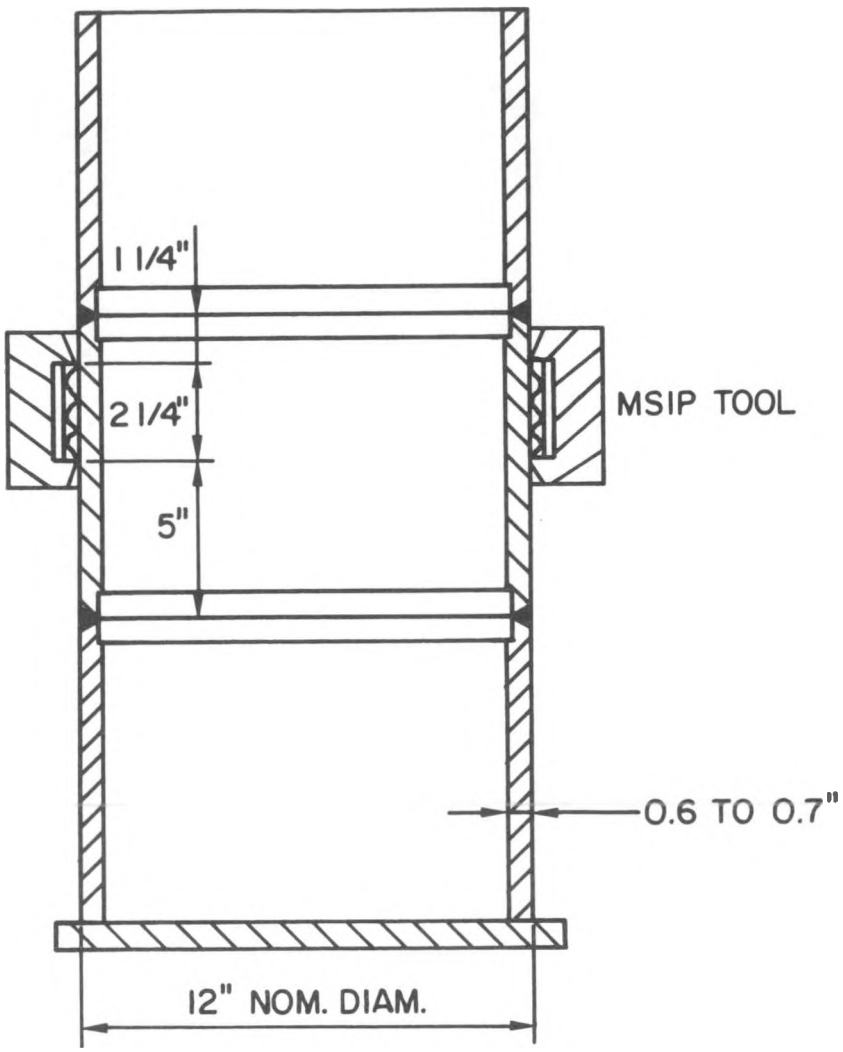

Fig. 1. Vermont Yankee 12-in.-diameter Specimen Treated by MSIP.

tool marks on the outer surface of the weldment are shown in Fig. 2. The lower weld is about 5 in. (125 mm) from the edge of the MSIP tool and would not be expected to receive the full benefit of the residual stress improvement expected from the process. The entire specimen was tested in boiling $MgCl_2$ at the J. A. Jones Applied Research Center in Charlotte, NC.

Shallow circumferential cracks were observed on the inner surface of the MSIP-treated weldment. The cracks were up to 120 μm deep and were located primarily in the fillet region at the end of the counterbore that was almost directly under the MSIP tool (Fig. 3). The crack morphology is transgranular and branched, and is consistent with chloride-induced SCC (Fig. 4). The same type of cracking was also observed in the fillet region

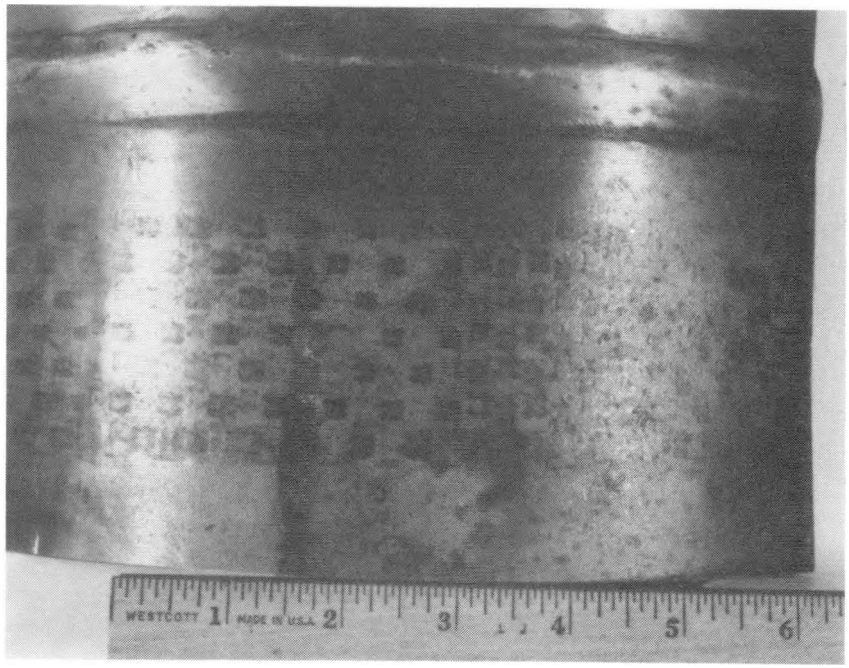

Fig. 2. MSIP Tool Marks at OD Surface of 12-in.-diameter Weldment.

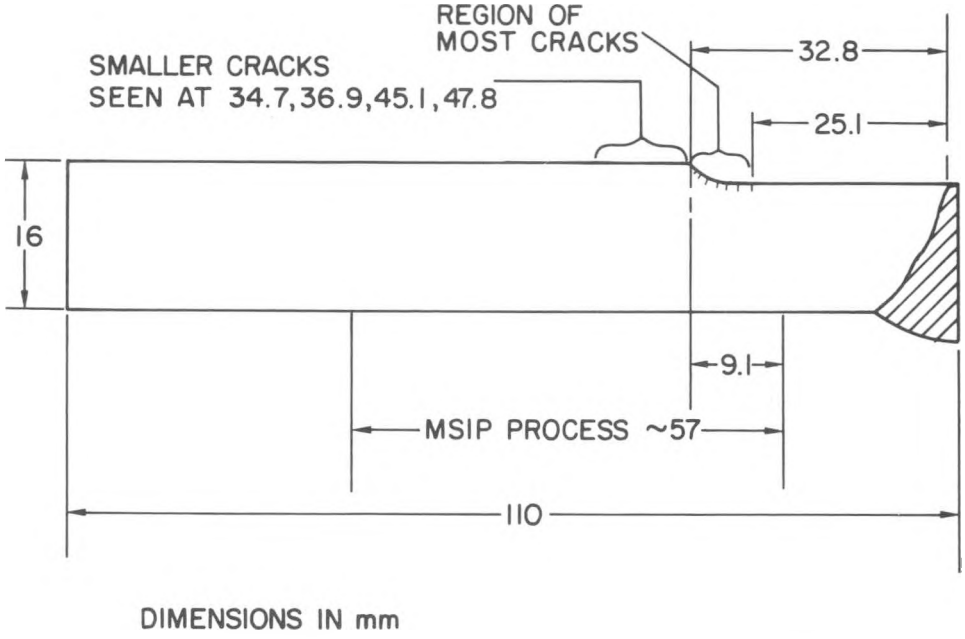

Fig. 3. Cracks at Fillet of Counterbore in 12-in.-diameter MSIP-Treated Weldment.

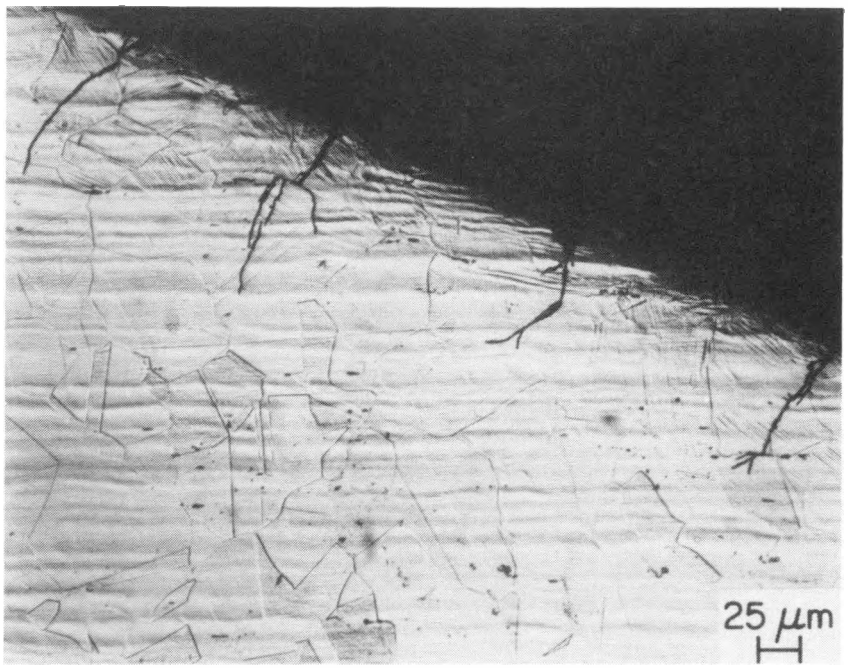

Fig. 4. Transgranular Cracks at the Inner Surface in the Fillet of the Counterbore almost Directly Beneath the MSIP Tool. Plastic deformation is evidenced by the slip lines within the grains.

at the end of the counterbore on the other side of the weldment (Fig. 5). The cracks are very tight and could not be observed by dye-penetrant tests with Magnaflux SKL-HF/S and SKD-NF/ZP-9B penetrants. They could be detected with Magnaflux DP-P1 penetrant and DP-D1 developer, although the cracks were too tight and shallow for the penetrant tests to be unambiguously interpreted without preknowledge of the existence of the cracks. These tests show that the circumferential cracks are 1-3 mm long.

In addition to the short, shallow, circumferential cracks in the fillet of the counterbore region of the MSIP-treated weldment, dye-penetrant tests and metallographic examination also revealed relatively deep (5.4 mm, 35% throughwall) circumferential cracks in the heat-affected zone (HAZ) of the second circumferential weld that was not MSIP-treated. The crack had propagated into the weld metal. The crack morphology is branched and transgranular, and appears consistent with chloride-induced SCC (Fig. 6). Dye penetrant tests also revealed long ($\sim$70 mm), longitudinal cracks on the inner surface of the pipe along the weld fusion line of the seam weld in the

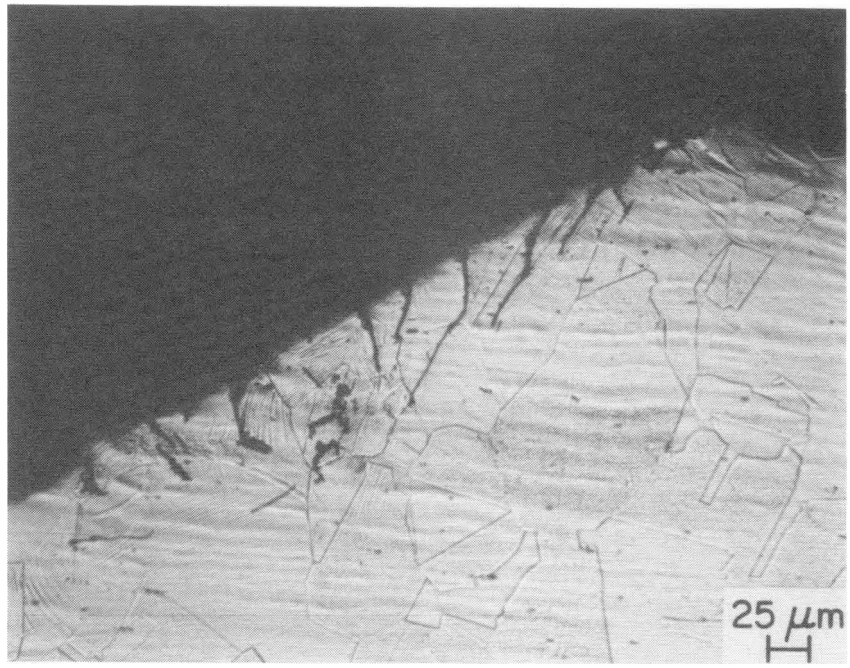

Fig. 5. Transgranular Cracks at the Inner Surface in the Fillet Region on the Other Side of the Weldment. Plastic deformation is evidenced by the slip lines within the grains.

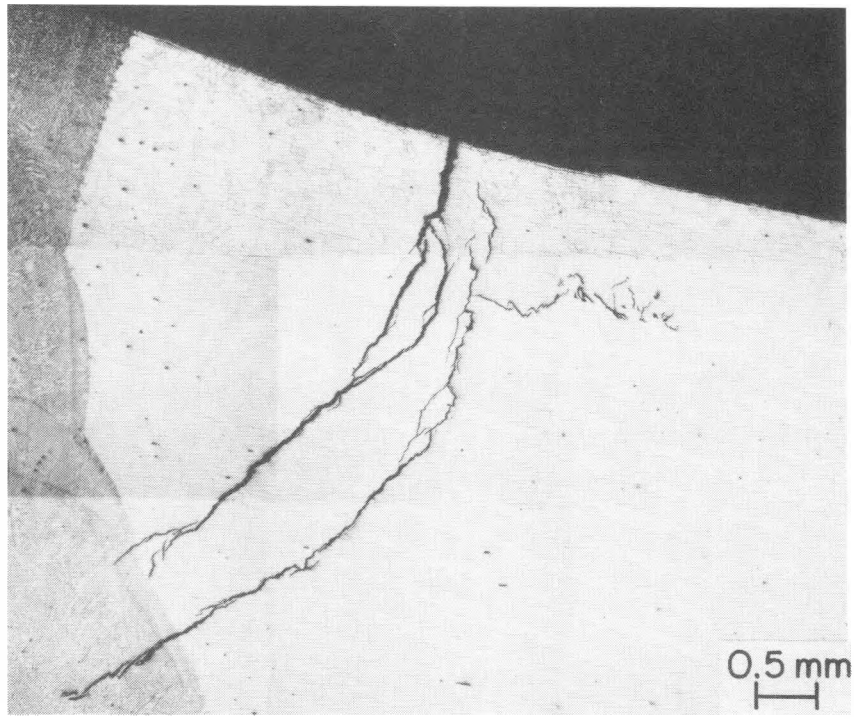

Fig. 6. Transgranular Cracks near an Untreated Weld.

region almost directly under the MSIP tool (Fig. 7). The remainder of the seam weld appears free of cracking. A cross section of the crack is shown in Fig. 8. At this section the crack is ∿3 mm deep (20% throughwall). The crack morphology is branched and transgranular and appears characteristic of chloride-induced SCC. The only cracks near the treated weld are the short, shallow cracks in the fillets at the ends of the counterbores.

According to the staff at J. A. Jones Applied Research, the area in which the cracks were found was checked by dye-penetrant tests both before and after the $MgCl_2$ tests, and no indications were observed. The cracks in the lower weld and the seam weld are now easily visible after dye-penetrant testing. However, large segments have been cut from the weldment, which relieved the residual stresses induced by the welding process and MSIP. This suggests that, as expected, the inner surface of the weldment was under high compressive residual stresses due to the MSIP process. This is consistent with the strain-gage residual stress measurements presented in the next section. Under these conditions it is unclear why $MgCl_2$ cracking should occur. At this point we can only conjecture that very local regions of tensile stress existed. Although the residual stresses measured in the second (lower) weld were compressive, this weld was ∿130 cm from the tool, and the induced stresses were not as compressive as in the treated weldment.

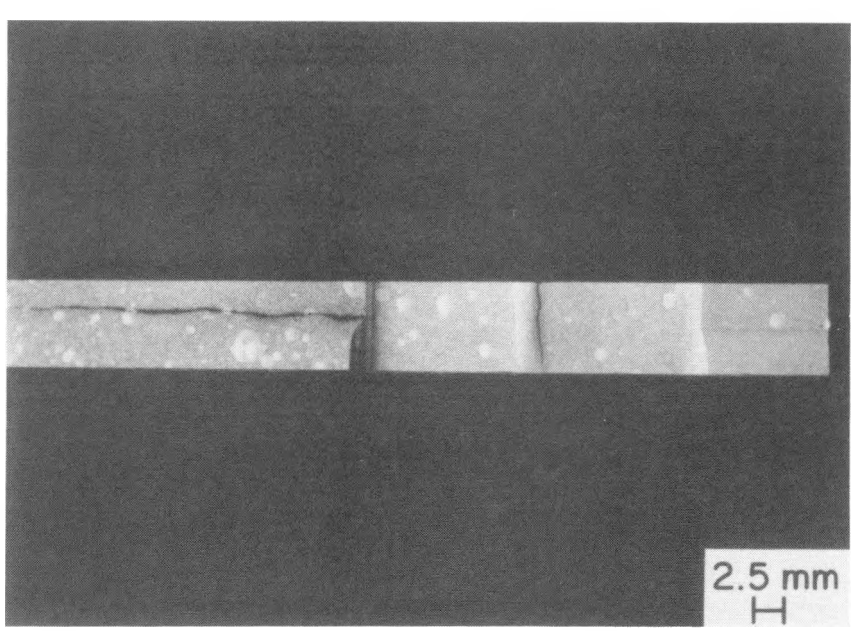

Fig. 7. Dye-penetrant Indications for the Seam Weld Crack.

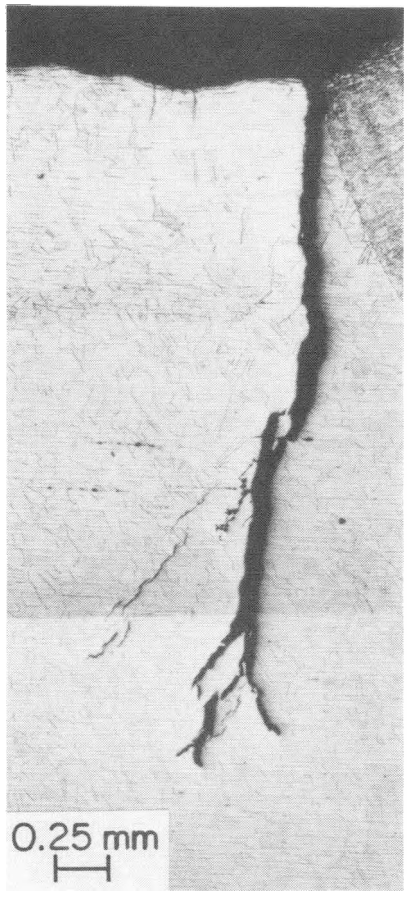

Fig. 8

Cross Section of
a Seam Weld Crack.

In the case of the crack in the fusion line of the seam weld, there appears to have been preexisting weld fusion flaws that could have provided a local stress riser. In the case of the shallow, tight cracks in the fillet of the counterbore of the treated weld, the tensile stresses were probably produced by the machining of the counterbore. Rough machining marks in the fillet region are shown in Fig. 9. The extreme tightness of the cracks suggests that the tensile stresses associated with them are highly localized with very steep throughwall gradients, which is characteristic of residual stresses produced by rough machining.

The reasons for the existence of the very local zones of tensile stress associated with the cracks are unlikely to be resolved completely. However, it does seem fair to state that the cracks were probably not caused by MSIP and that the favorable residual stress state produced by MSIP greatly reduced the amount of cracking that would have been observed in

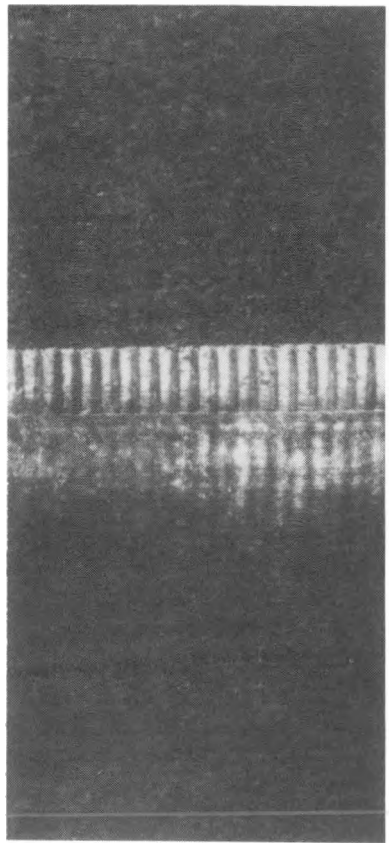

Fig. 9

Machining Marks at the Fillet of Counterbore.

a corresponding untreated weldment subjected to a similar $MgCl_2$ test. A 28-in.-diameter weldment that has been treated by MSIP is currently being examined. This weldment was not tested in $MgCl_2$, and the absence of cracking in this weldment would confirm that the observed cracking in the 12-in.-diameter weldment is due to the $MgCl_2$.

b. Measurements of the Residual Stresses Associated with the Mechanical Stress Improvement Process (W. J. Shack)

Residual stress measurements were made on the 12-in.-diameter pipe weldment. The stresses on the inner surface were measured at two azimuthal positions. There are some variations between the two sets of measurements, but the results are qualitatively and quantitatively similar. At one azimuth, throughwall stress measurements were made at six axial positions ranging from the HAZs on both sides of the weld to the region directly under the tool.

The welds in the pipe segment were prepared by Morris-Knudsen Co. under the sponsorship of Vermont Yankee Nuclear Power Corp. using standard nuclear industry practice. No control welds were prepared, but calculations and measurements on such welds suggest that the axial stresses in the HAZs of such welds will typically be tensile with a magnitude of ∿20-30 ksi.

The process appears to have been very successful. Strongly compressive stresses (-30 to -50 ksi) were induced on the inner surface in the HAZ of the treated weld. Although analytical results by OAI suggest that there will be tensile stresses on the inner surface in the region directly under the tool, the measured stresses were compressive (approximately -15 ksi). Overall, the stress patterns produced by MSIP appear comparable with those produced by IHSI. Although as shown in Fig. 1, the second (lower) weld is ∿5 in. from the edge of the tool, it also appears to have much lower stress levels than would be expected. The stresses measured by the strain gage technique are consistent with the results of the $MgCl_2$ tests, i.e., except for the isolated cracks discussed previously, no cracking was observed in the vicinity of the two welds.

The MSIP process parameters used by OAI are summarized in Table 1. The geometric distortions introduced by the process, as measured by OAI, are summarized in Fig. 10. These values are consistent with check measurements made at ANL. Although the reported strains seem modest, the distortion introduced by the process is quite evident.

The locations for the stress measurements are indicated in Fig. 11. The two azimuthal positions were 90° apart and are denoted as 0° and 90° in the figures and tables. At the 0° azimuth, strain-gage rosettes (Micro Measurement EA-09-030YB-120) were laid at nine locations on the inner surface close to the upper weld and at four locations close to the lower weld. At the 90° azimuth, seven rosettes were laid near the upper weld and four near the lower weld. After the gages were laid, full-length bar sections approximately two inches wide containing the strain gages were cut from the pipe segment. The bars were shortened, and the gages on the inner surface were completely stress relieved by cutting a thin slab (∿2 mm thick) from the inner surface by wire-cut electric-discharge machining (EDM).

TABLE 1. MSIP Parameters for Vermont Yankee 12-in.-diameter Weldment

	Applied
Use of standard MSIP 12-in. tool	One-sided
Flexible pad width	2-1/4 in.
Distance from weld centerline	1-1/4 in.
Radial contraction measured at the sides of pressure band (flexible pad)	0.94%[a] 0.96%[b]
Radial contraction at midplane of pressure band	1.41%
Radial contraction at weld on tool side	0.47%
Gap closing between 2000 psi initial load and final load	0.683 in.[d]

[a]Weld side.
[b]Pipe side.
[c]Use of 0.125-in. shims on both sides was required.
[d]Shims inserted after reaching 9000 psi; the final tensioner applied 12,000 psi.

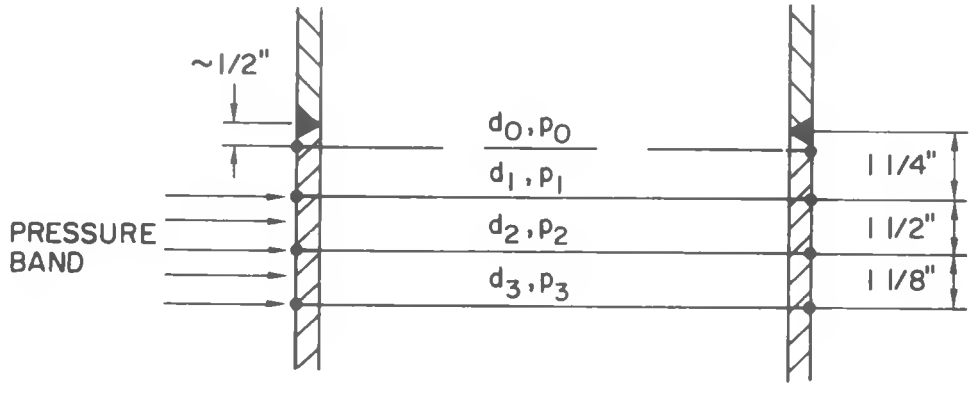

Fig. 10. Pipe Dimensions before and after MSIP.

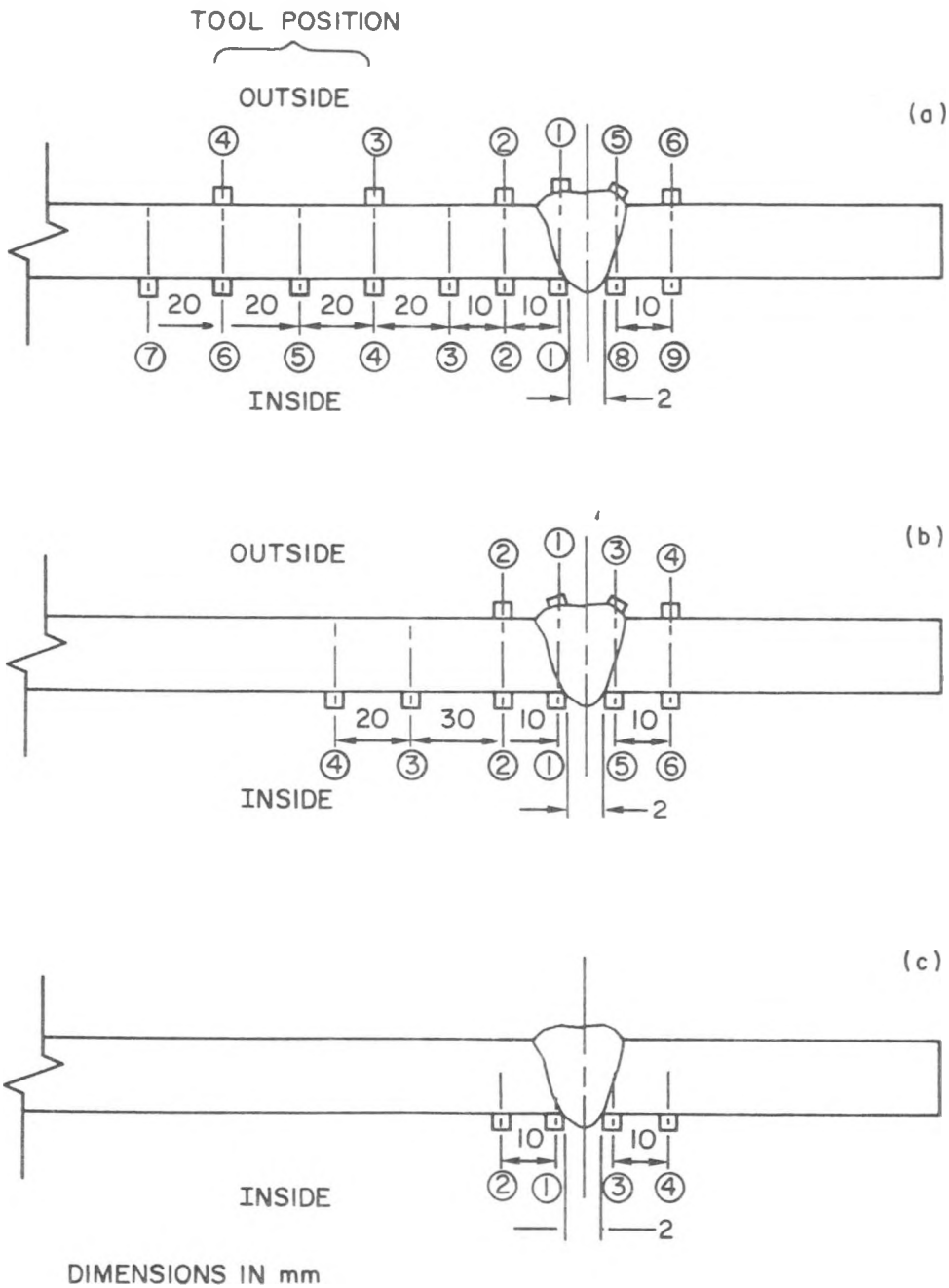

Fig. 11. Strain Gage Locations on the 12-in.-diameter MSIP Weldment. (a) 0° Azimuth Upper MSIP-treated Weld, (b) 90° Azimuth Upper MSIP-treated Weld, (c) 0° Azimuth Untreated Lower Weld.

The measured residual stresses on the inner surface near the upper MSIP-treated weld are summarized in Table 2 for the two azimuths examined. Both the axial and hoop stresses are compressive at all locations. As noted previously, finite-element analyses by OAI predict tensile stress regions on the portion of the inner surface directly beneath the tool. In the present case, the stresses are compressive in this region (gages 4, 5, and 6 for the 0° azimuth; gages 3 and 4 for the 90° azimuth), although the stresses are not as compressive as they are closer to the weld. The one-sided tool appears to be effective in introducing compressive stresses in the HAZs on both sides of the treated weld. In fact, in this particular case, the stresses are more compressive on the far side of the weld at both azimuths. (It is not clear why this occurs. The gages are not close to any geometric stress raisers; however, it may be that the two sides of the weld have somewhat different thermomechanical histories and hence somewhat different plastic stress-strain behavior.)

The measured residual stresses on the inner surface near the lower weld are summarized in Table 3. With the exception of the hoop stress at gage position 2 at the 0° azimuth, all the measured stresses are compressive. This is consistent with the boiling $MgCl_2$ test, which showed only very localized cracking. Since the welds were made with conventional welding practice (i.e., without heat-sink cooling), prior experience and analysis suggest that the inner surface stresses in the HAZ should be tensile in the as-welded condition. Hence, the compressive stresses are probably due to MSIP, even though the edge of the tool is ∿5 in. from the centerline of this weld.

The throughwall measurements were made at the 0° azimuth and are always referred to in terms of the gage positions on the outer surface. The locations of these gages and the corresponding gages on the inner surface are summarized in Table 4.

The throughwall stress measurements were made by monitoring the strain changes on the outer surface as thin (1.6 mm) layers were machined from the inner surface after the thin slab containing the strain gages on the inner surface was removed by EDM. The strains that are relieved on the inner and outer surfaces can be measured directly; however, the strains (stresses) in the

TABLE 2. Measured Residual Stresses for a 12-in.-diameter Pipe Weldment Treated by the Mechanical Stress Improvement Process (0° Azimuth)

(0° Azimuth)

Gage Position	Distance From Weld Centerline, in.	Axial Stress, ksi	Hoop Stress, ksi
1	-0.20	-33	-33
2	-0.59	-35	-23
3	-0.99	-26	-13
4	-1.77	-16	-15
5	-2.57	-13	-14
6	-3.35	-14	-15
7	-4.14	-17	-13
8	0.20	-31	-36
9	0.59	-44	-33

(90° Azimuth)

Gage Position	Distance From Weld Centerline, in.	Axial Stress, ksi	Hoop Stress, ksi
1	-0.20	-30	-36
2	-0.59	-36	-30
3	-1.77	-17	-19
4	-2.57	-17	-21
5	0.20	-38	-36
6	0.59	-51	-30

interior of the pipe wall are determined indirectly with the assumption that the stress redistribution across the remaining thickness is linear as each layer is removed. Although this is not rigorously true, comparison with more exact elastic solutions shows that it is a good approximation for the stress distributions typical of thickwall pipe weldments.[1]

Complete throughwall measurements were made at gage positions 2, 3, 4, and 6. Gage failures occurred at positions 1 and 5 after approximately one-half of the wall was removed, so only partial information is available at these positions. The axial throughwall stress profiles at each position are shown in Figs. 12-14 as a function of the nondimensional depth (the inner surface is at 0, the outer surface at 1). The actual experimental measurements

TABLE 3. Measured Residual Stresses at the Lower Weldment ~5 in. from the MSIP Tool

(0° Azimuth)

Gage Position	Distance From Weld Centerline, in.	Axial Stress, ksi	Hoop Stress, ksi
1	-0.20	-5	-2
2	-0.59	-11	4
3	0.20	-7	-10
4	0.59	-5	-9

(90° Azimuth)

Gage Position	Distance From Weld Centerline, in.	Axial Stress, ksi	Hoop Stress, ksi
1	-0.20	-12	-16
2	-0.59	-27	-13
3	0.20	-9	-21
4	0.59	-21	-20

TABLE 4. Gage Locations for Throughwall Stress Measurements on the 12-in.-diameter Weldment

Gage Position on Outer Surface	Distance From Weld Centerline, in.	Corresponding Gage Position on Inner Surface
1	-0.20	1
2	-0.59	2
3	-1.77	4
4	-3.35	6
5	0.20	8
6	0.59	9

are shown as discrete points. At locations where complete throughwall profiles were obtained, a fourth-order polynomial fit to the data was made, and the results are represented by solid curves in the figures.

In the regions near the HAZs (gage positions 2 and 6), the distributions are almost linear across the thickness except near the outer surface. They are similar to the profiles obtained from measurements on 12-in.-diameter pipe weldments treated by IHSI, although the profiles obtained by finite-element

calculations that model the IHSI process are more nonlinear.[2] In the region directly under the tool the profiles are also very nonlinear. The actual data at gage positions 3 and 4 are more nonlinear than is indicated by the fitted curves, since a tensile "nose" occurs at a depth of ∿0.35 in. that is not well represented by the polynomial interpolation.

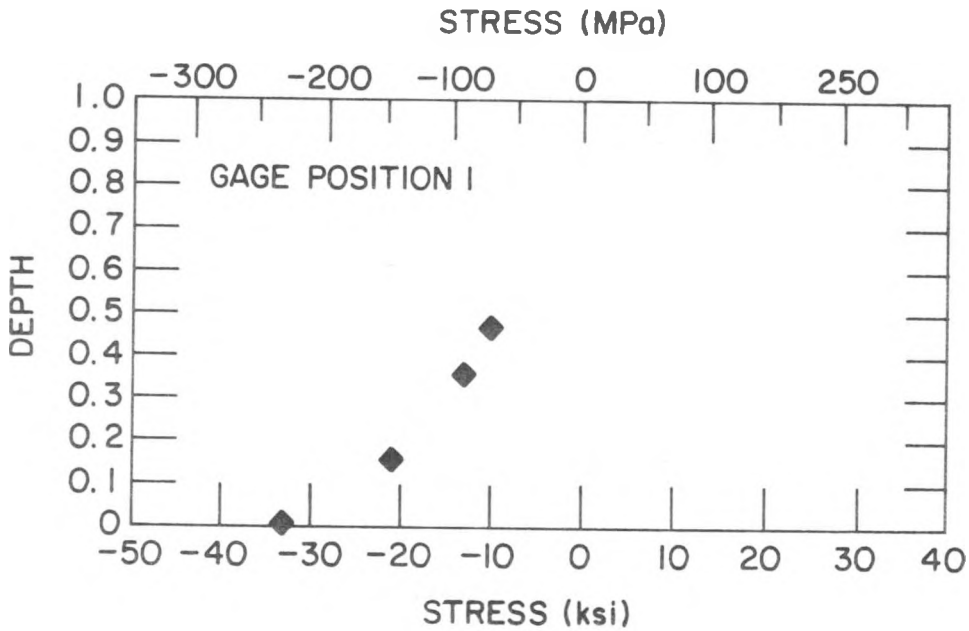

(a)

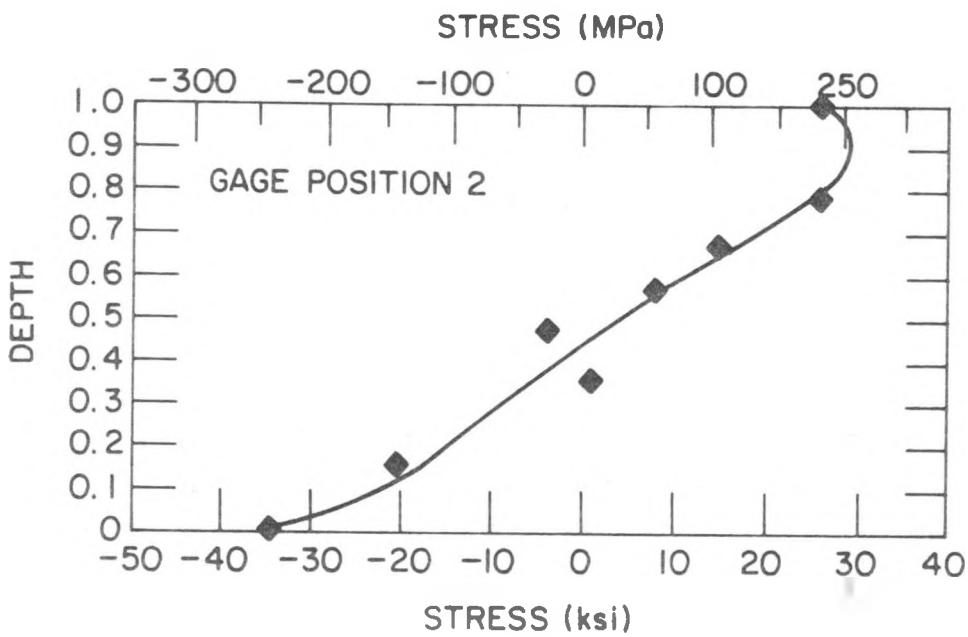

(b)

Fig. 12. Throughwall Axial Residual Stresses in the HAZ next to the MSIP Tool. (a) Gage Position 1 and (b) Gage Position 2.

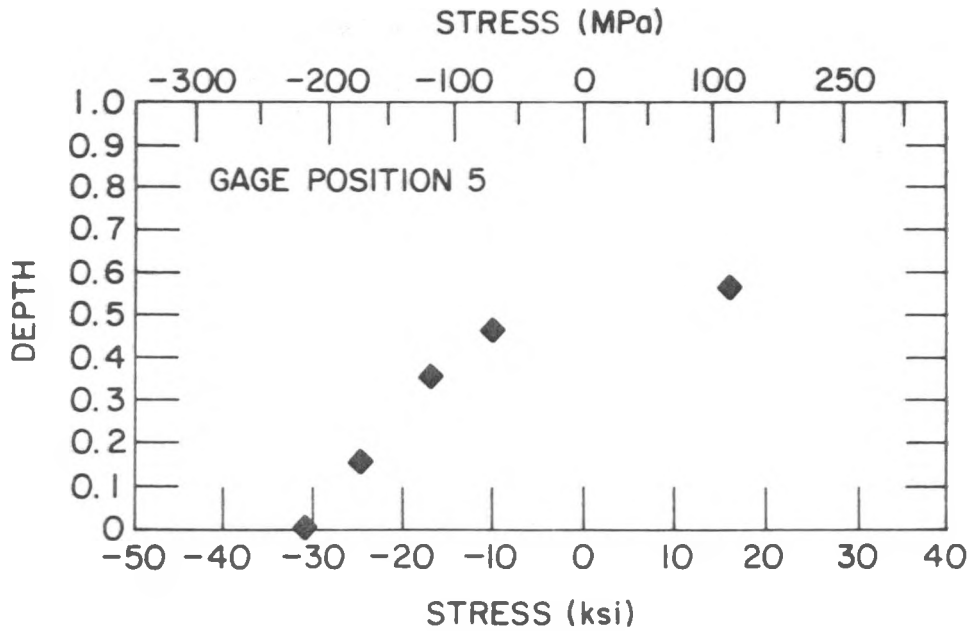

(a)

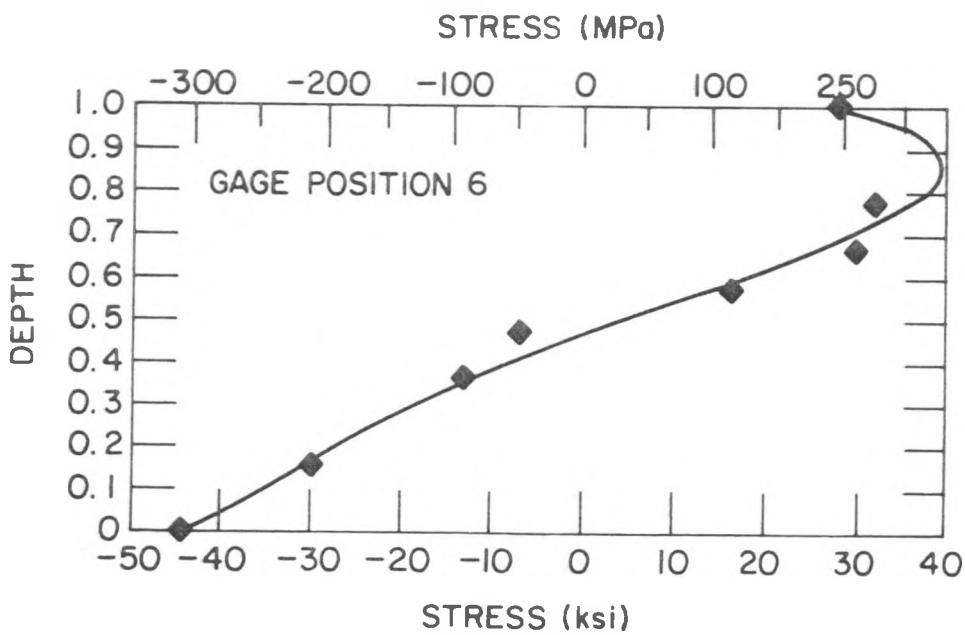

(b)

Fig. 13. Throughwall Axial Residual Stresses in the HAZ across the Weld from the MSIP Tool. (a) Gage Position 5 and (b) Gage Position 6.

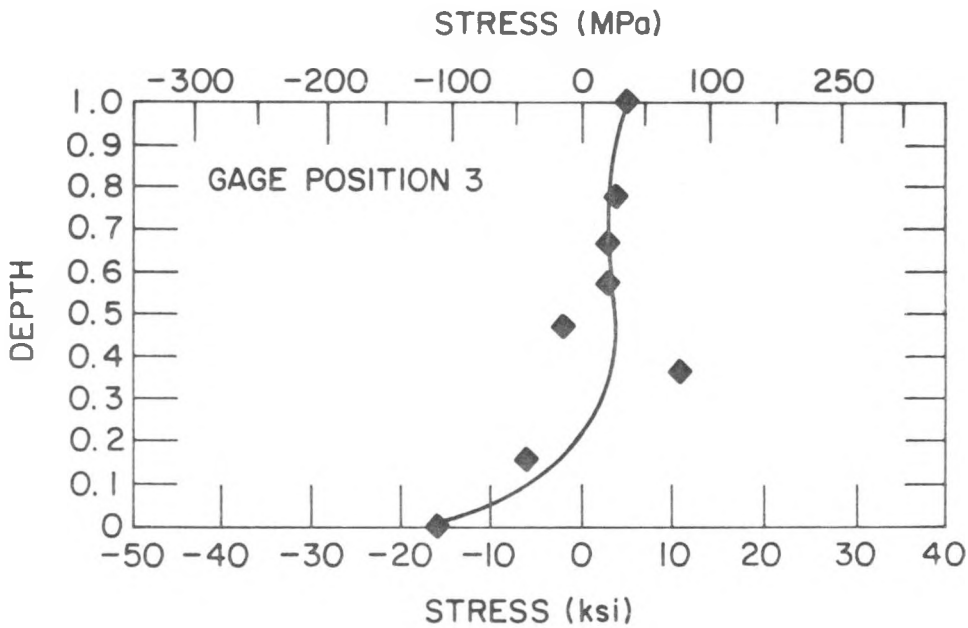

(a)

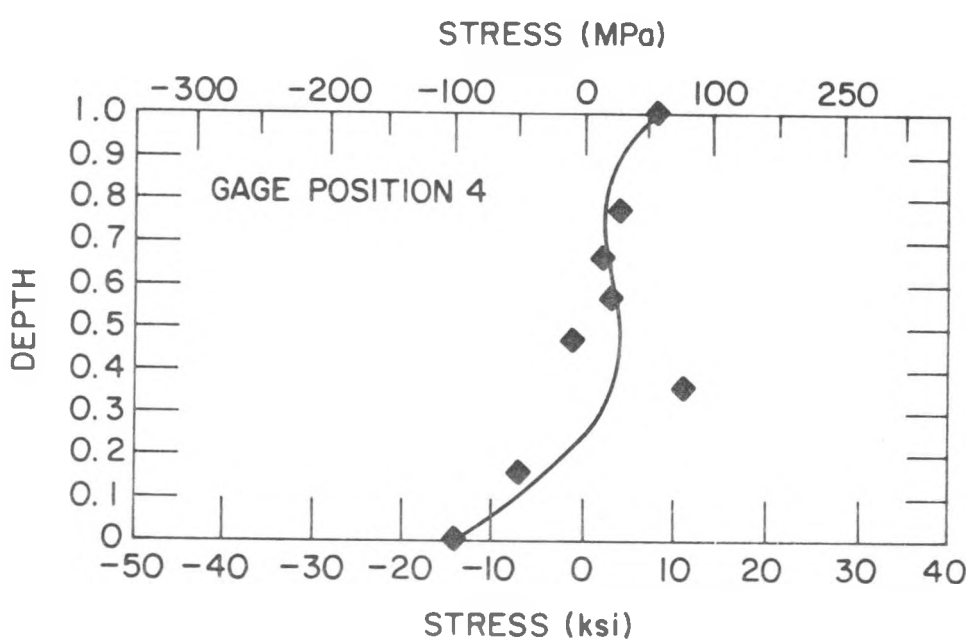

(b)

Fig. 14. Throughwall Axial Residual Stresses in the Region under the MSIP Tool. (a) Gage Position 3 and (b) Gage Position 4.

B. Evaluation of Nonenvironmental Corrective Actions (P. S. Maiya and W. J. Shack)

1. Introduction

The fundamental premise of the current efforts to prevent IGSCC in boiling-water reactor (BWR) piping is that IGSCC involves complex interactions among material susceptibility (sensitization), the stress acting on the material, and the environment; and that suitable alteration or variation of these parameters can produce immunity to IGSCC. Nonenvironmental corrective actions seek to mitigate either the material susceptibility or the state of stress on the inside surface of weldment. They include techniques for improving the margin against IGSCC of a susceptible material like Type 304 SS and the identification of alternative materials that are inherently more resistant to IGSCC.

The objective of the current work is an independent assessment of proposed remedies developed by the utilities and the vendors. Additional testing and research have been carried out to eliminate gaps in the existing data base on alternative materials and fabrication, and to develop a better understanding of the relation between the existing laboratory results and satisfactory in-reactor operating performance.

2. Technical Progress

a. SCC Susceptibility of German TP 347 SS

In a cooperative effort with the Electric Power Research Institute (EPRI) Non-Destructive Examination (NDE) Center, SCC susceptibility studies are being carried out on the German TP 347 SS. TP 347 SS has been used in both pipe and clad forms in German pressurized-water reactors (PWRs) and BWRs with no reported stress corrosion problems. The tests are being performed on weldments fabricated at the EPRI NDE center using a matching filler material. The initial CERT tests are intended to evaluate the effects of dissolved-oxygen and impurity concentration and strain rate on SCC susceptibility in high-temperature water. Additional tests are planned to evaluate

the crack growth resistance of the material under crevice conditions. The chemical compositions of the base and filler materials currently being tested are listed in Table 5.

TABLE 5. Chemical Analysis (wt %) of Different Heats of Nuclear Grade Type 347 SS

Element	No. 174100	No. 170162	No. 90316[a]
Si	0.33	0.43	0.80
Mn	1.70	1.70	1.61
C	0.023	0.03	0.017
P	0.036	0.012	0.018
S	0.015	0.019	0.002
Ni	11.0	10.75	10.85
Cr	18.15	18.53	19.53
Mo	0.48	0.35	0.03
Nb	0.44	0.51	0.61
Cu	0.12	0.11	0.04
Mg	0.005	0.005	-
N	0.029	0.0212	-
O	0.0046	0.0037	-
B	0.0005	0.0005	-
Co	-	-	0.03
Fe	Balance	Balance	Balance

[a]Filler metal (welded at the EPRI NDE Center).

The filler material (Heat No. 90316) is of matching chemistry to the base materials. The ferrite contents of the welds applied to Heat Nos. 174100 and 170162 of the base materials are 7.9 and 6.3 vol %, respectively, as measured with a ferrite scope. This difference is not considered significant. The grain size of the two base materials is shown in Table 6.

TABLE 6. Grain Size Variation in the Two Heats of Nuclear-Grade Type 347 SS[a]

Heat No.	Mean Grain Intercept Dia., μm	ASTM Grain Size No.
174100	17.9	8.2
170162	34.8	6.3

[a]After a heat treatment of 500°C/24 h.

The CERT tests were performed on material in the as-welded condition and after an additional heat treatment (i.e., as-welded plus 500°C/24 h) over a range of strain rates in 289°C water with ∿0.25 ppm dissolved oxygen and 0.1 ppm sulfate. The results are given in Table 7. Average crack growth rates were estimated in a manner similar to that used for Type 316NG and other materials.[3] Both scanning electron microscopy (SEM) and optical metallographic examinations were performed on a few specimens in the vicinity of the weld/base-metal interface to determine susceptibility to classical "knife-line attack."

TGSCC occurs at a strain rates of $<5 \times 10^{-7}$ s^{-1}. This critical strain rate is slower than that required to produce transgranular stress corrosion cracking (TGSCC) in CERT tests on Type 316NG SS. However, the average crack growth rates for TP 347 SS are slightly higher than those determined for Type 316NG SS (Table 8). Failure always occurred in the base metal and there was no evidence of any "knife-line attack." The effect of the "low-temperature sensitization" ("LTS") heat treatment on SCC is not significant in a low-carbon material, as expected.

TABLE 7. CERT Test Results for Type 347 Stainless Steel in 289°C Water Containing ∿0.23 ppm Oxygen and 0.1 ppm Sulfate[a]

Specimen No.	Heat Treatment	$\dot{\varepsilon}$, s^{-1}	t_f, h	ε_f, %	ε_u, %	$\Delta A/A_o$, %	σ_{max}, MPa	Failure Mode	$\dot{a}_{av}$, $m \cdot s^{-1}$
174-1	b	1×10^{-6}	77.5	27.9	19.4	62	435	Ductile	-
174-4	c	1×10^{-6}	65.5	23.6	18.2	65	432	Ductile	-
174-2	b	5×10^{-7}	136.6	24.6	19.0	51	428	TGSCC	1.40×10^{-9}
174-5	c	5×10^{-7}	114.5	20.6	16.6	47	417	↓	1.63×10^{-9}
174-8	b	2×10^{-7}	328.5	23.7	19.9	41	434	↓	1.00×10^{-9}
174-3	c	2×10^{-7}	301.5	21.7	17.8	40	448	↓	1.10×10^{-9}
174-9	b	1×10^{-7}	676.5	24.4	21.6	41	443	↓	1.05×10^{-9}
174-6	c	1×10^{-7}	574.5	20.7	16.4	47	451	↓	7.58×10^{-10}

[a]Steady-state open-circuit corrosion potential: ∿30 mV(SHE).
[b]As welded.
[c]As welded plus 500°C/24 h.

TABLE 8. Average Crack Growth Rates for Nuclear-Grade Type 347 and Type 316NG Specimens[a] in 289°C Water Containing 0.25 ppm Oxygen and 0.1 ppm Sulfate

$\dot{\varepsilon}$, s^{-1}	$\dot{a}_{av}$, m s^{-1}	
	347[b]	316NG[c]
5×10^{-7}	1.52×10^{-9}	1.05×10^{-9}
2×10^{-7}	1.05×10^{-9}	7.35×10^{-10}
1×10^{-7}	9.04×10^{-10}	6.73×10^{-10}

[a]After heat treatment of 1050°C/0.5 h plus 650°C/24 h.
[b]Heat No. 174100.
[c]Heat No. P91756.

Experiments at lower impurity (i.e., sulfate) concentrations indicate that a transition from transgranular cracking to a ductile failure mode occurs in TP 347 SS, although the critical concentration depends on the strain rate (Table 9). Results on another heat of TP 347 SS (Heat No. 170162) are summarized in Table 10; they are similar to those observed for Heat No. 174100. TGSCC occurs in impurity environments at a critical strain rate of a 5×10^{-7} s^{-1}.

The results at a strain rate of 2×10^{-7} s^{-1} for the two heats of material are conveniently summarized on a water chemistry diagram described by the conductivity (determined by the impurity species) and the open-circuit corrosion potential of the steel (principally determined by the dissolved oxygen content) as shown in Fig. 15. The corresponding results for our reference heat of Type 316NG SS are shown in Fig. 16. Both Types TP 347 and 316NG SS appear to have a relatively small tolerance to impurities in the oxygenated water.

The TGSCC susceptibility of the austenitic stainless steels observed in CERT tests is not surprising in view of some qualitative mechanistic considerations. A number of the alloying elements common to austenitic

TABLE 9. Effect of Dissolved Oxygen and Sulfate on SCC Susceptibility of Type 347 SS in 289°C Water

Test No.	Heat Treatment	Oxygen, ppm	Sulfate, ppm	SS Potential (mV)SHE	$\dot{\varepsilon}$, s^{-1}	t_f, h	ε_f, %	$\Delta A/A_o$, %	σ_{max}, MPa	Failure Mode	$\dot{a}_{av}$, $m \cdot s^{-1}$
265	a	0.22	0.1	75	5×10^{-7}	136.6	24.6	51	428	TGSCC	1.40×10^{-9}
274	b	0.25	0.1	93	5×10^{-7}	114.5	20.6	47	417	TGSCC	1.63×10^{-9}
283	b	0.21	0.05	53	5×10^{-7}	126.3	22.7	70	435	Ductile	-
276	a	0.25	0.1	34	2×10^{-7}	328.5	23.7	41	434	TGSCC	1.00×10^{-9}
272	b	0.27	0.1	2	2×10^{-7}	301.5	21.7	40	448	TGSCC	1.10×10^{-9}
285	b	0.28	0.05	35	2×10^{-7}	280.7	20.2	47	458	TGSCC	8.31×10^{-10}
288	b	0.26	0	-39	2×10^{-7}	313.5	22.6	78	442	Ductile	-

[a] As-welded.
[b] As-welded plus 500°C/24 h.

TABLE 10. CERT Test Results for Type 347NG SS at 289°C

Test No.	Oxygen, ppm	Sulfate, ppm	SS Potential, mV (SHE)	$\dot{\varepsilon}$, s^{-1}	t_f, h	ε_f, %	$\Delta A/A_o$, %	σ_{max}, MPa	a_{av}, $m \cdot s^{-1}$
301	0.25	0.1	84	1×10^{-6}	55.7	20.1	76	427	0
305	0.25	0.1	91	5×10^{-7}	114.1	20.5	67	430	b
297	0.26	0	22	2×10^{-7}	253.8	18.3	80	444	0
310	0.25	0.1	22	2×10^{-7}	250.5	18.0	61	471	5.5×10^{-10}
299	0.005	0.025	-609	2×10^{-7}	243.2	17.5	54	438	3.5×10^{-10}
304	0.005	0.05	-580	2×10^{-7}	231.8	16.7	69	442	4.6×10^{-10}

[a] Heat No. 170162.
[b] Evidence of initiation, but the crack length is too short to estimate a velocity.

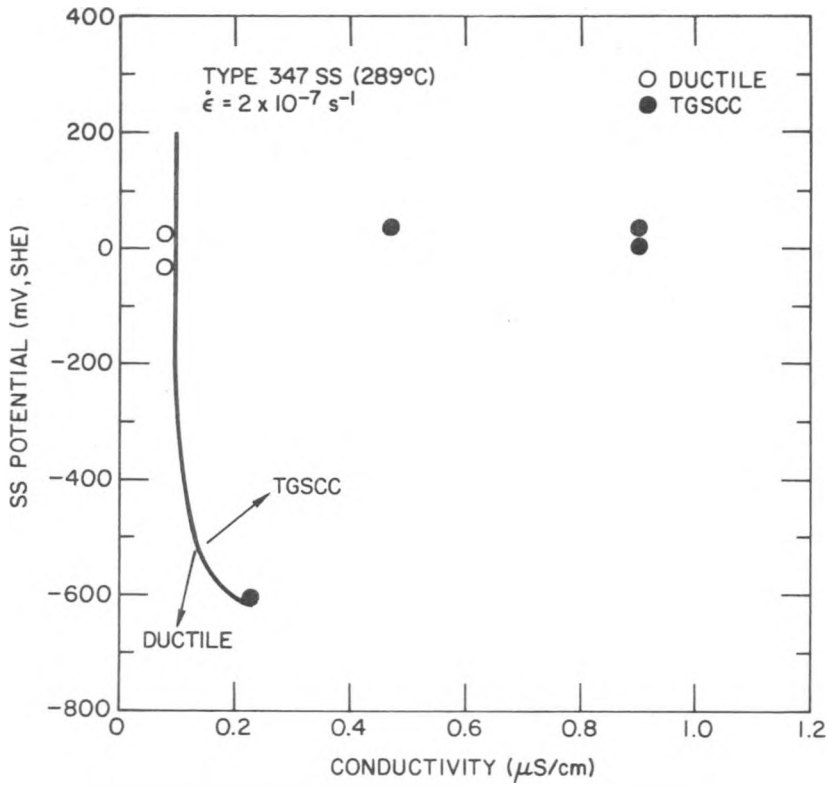

Fig. 15. Influence of Open-Circuit Corrosion Potential and Water Conductivity on the Fracture Mode of Type 347NG SS in CERT Experiments in 289°C Water Containing Dissolved Oxygen and Sulfate.

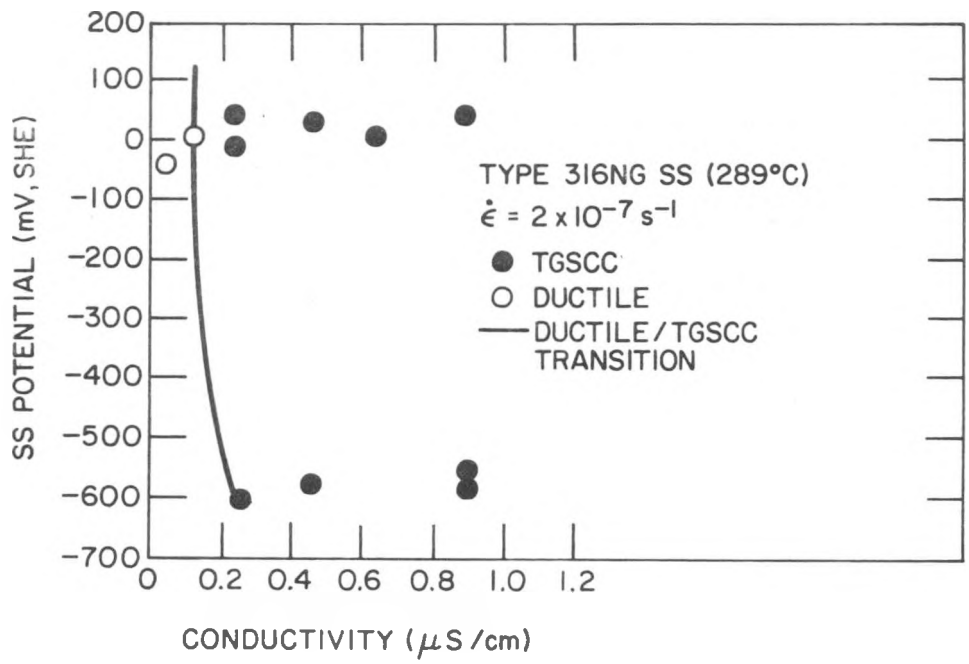

Fig. 16. Influence of Open-Circuit Corrosion Potential and Water Conductivity on the Fracture Mode of Type 316NG SS in 289°C Water Containing Dissolved Oxygen and Sulfate.

stainless steels such as Cr, Mo, Nb, and Ti are known to lower the stacking fault energy, which promotes slip planarity. Alloys in which dislocations move on the same slip planes with little cross slip are most susceptible to TGSCC.[4,5] Although the reasons for this behavior are not clear, it is believed that slip planarity promotes the film rupture process involved in SCC.

b. Phenomenological Models for SCC

We have presented a model based on simplified elastic-plastic fracture mechanics analysis of a CERT specimen and a slip-dissolution mechanism for crack advance[6,7] that can be used to account for strain rate, environmental, and microstructural effects on SCC in CERT tests. The prediction of this model can be written in generalized form as

$$P = A^{p}(J_c/C)^{q}(\dot{\varepsilon})^{r} \qquad (1)$$

where

P = SCC susceptibility parameter (e.g., ε_f, a_f, t_f, or $\dot{a}_{av}$),
ε_f = failure strain,
a_f = intergranular or transgranular crack length,
t_f = time to failure,
a_{av} = average crack growth rate $\simeq (a_f - a_o)/(t_f - t_o)$,
a_o, t_o = crack initiation length and time, respectively,
A = parameter which is a function of dissolved oxygen, corrosion potential, and material microstructural variables,
J_c/C = fracture-characterizing parameter which depends on the geometry and material but is almost independent of environment,

and

p, q, and r are given by the model.

The approximate constancy of J_c/C [or more precisely, the dimensionless parameter $J_c/(C_o a_o)$] is demonstrated in Fig. 17. The data in this figure are based on tests for Type 304 SS in which the conductivity and

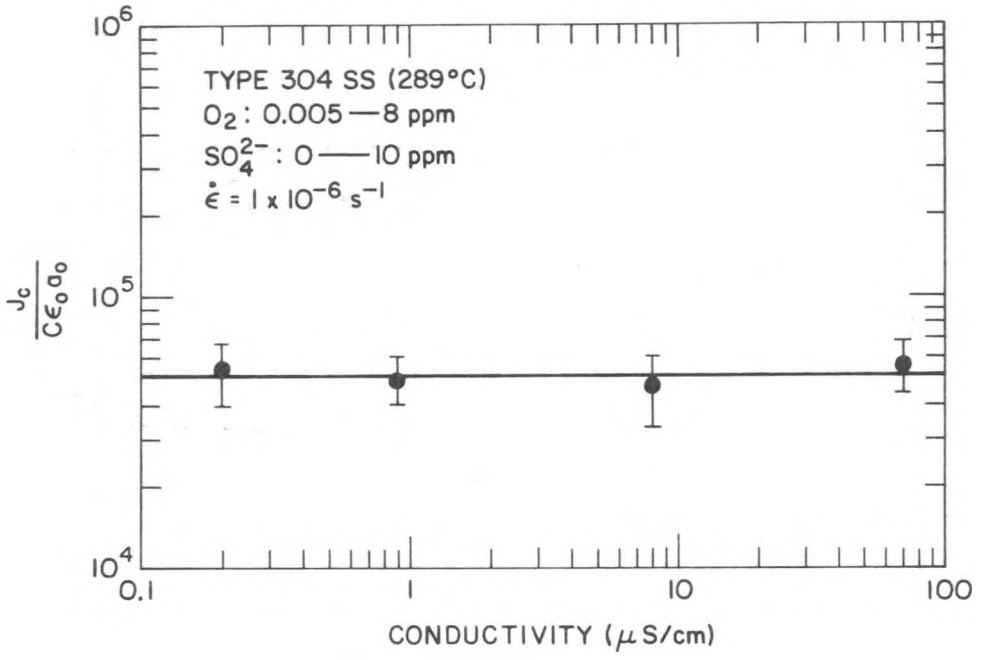

Fig. 17. Fracture Characterizing Parameter versus Water Conductivity for Type 304 SS. The vertical bar shows the effect of dissolved oxygen or corrosion potential on the fracture characterizing parameter.

dissolved-oxygen concentration of the feedwater have been varied by nearly three orders of magnitude.[8] The degree of sensitization (DOS) of the steel, as quantified by the electrochemical potentiokinetic reactivation (EPR) technique, was varied from 2 to 30 C/cm^2.

The dependence of the parameter A on dissolved-oxygen level, open-circuit corrosion potential, and DOS for high-purity water and impurity environments is shown in Figs. 18-22. The variation of A and $\dot{a}_{av}$ with nitrogen content of the above alloys is shown in Fig. 23. Nitrogen is believed to play an important role in promoting planar slip and, hence, sensitivity to TGSCC. Caution should be used in extrapolating beyond the range of nitrogen levels covered in Fig. 23, since there is some indication that nitrogen is detrimental only at concentrations >0.10 wt %, as shown in Fig. 24.

The specific relationship between the crack growth rate $\dot{a}_{av}$ and the strain rate $\dot{\epsilon}$ predicted by the model for CERT tests carried to failure is

$$\dot{a}_{av} = A(AC/J_c)^{1/3}\dot{\epsilon}^{1/3} \quad . \tag{2}$$

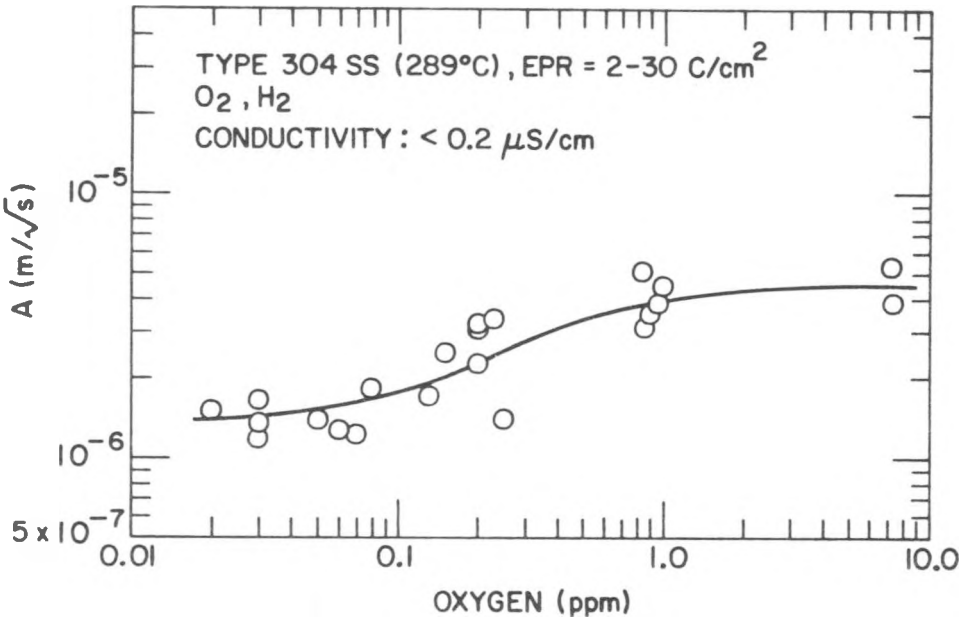

Fig. 18. Variation of A with Dissolved Oxygen in High-Purity Water.

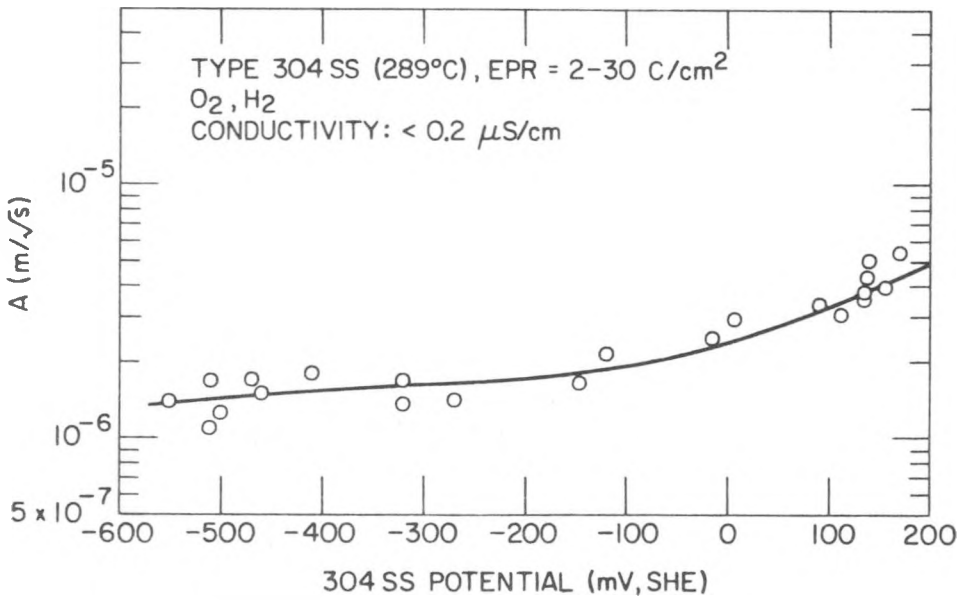

Fig. 19. Variation of A with Open-Circuit Corrosion Potential in High-Purity Water.

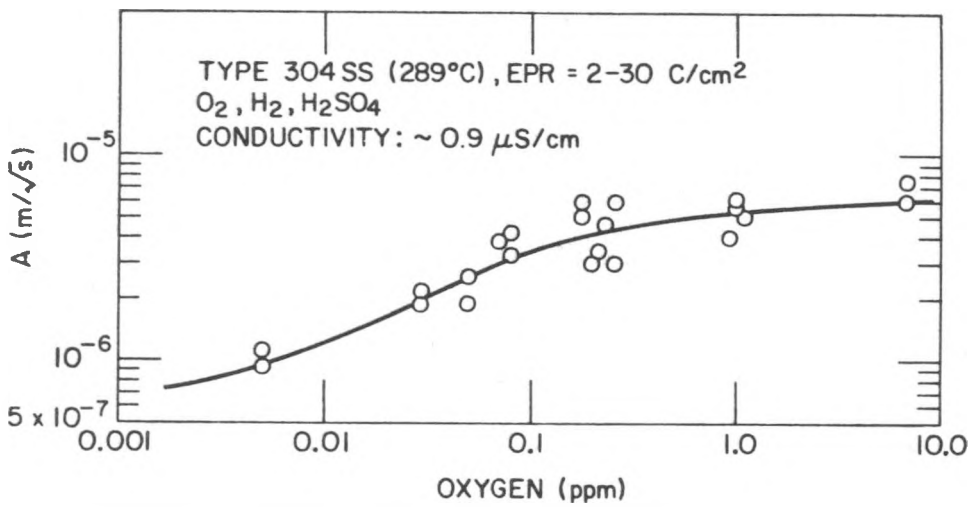

Fig. 20. Variation of A with Dissolved Oxygen in Water Containing 0.1 ppm Sulfate.

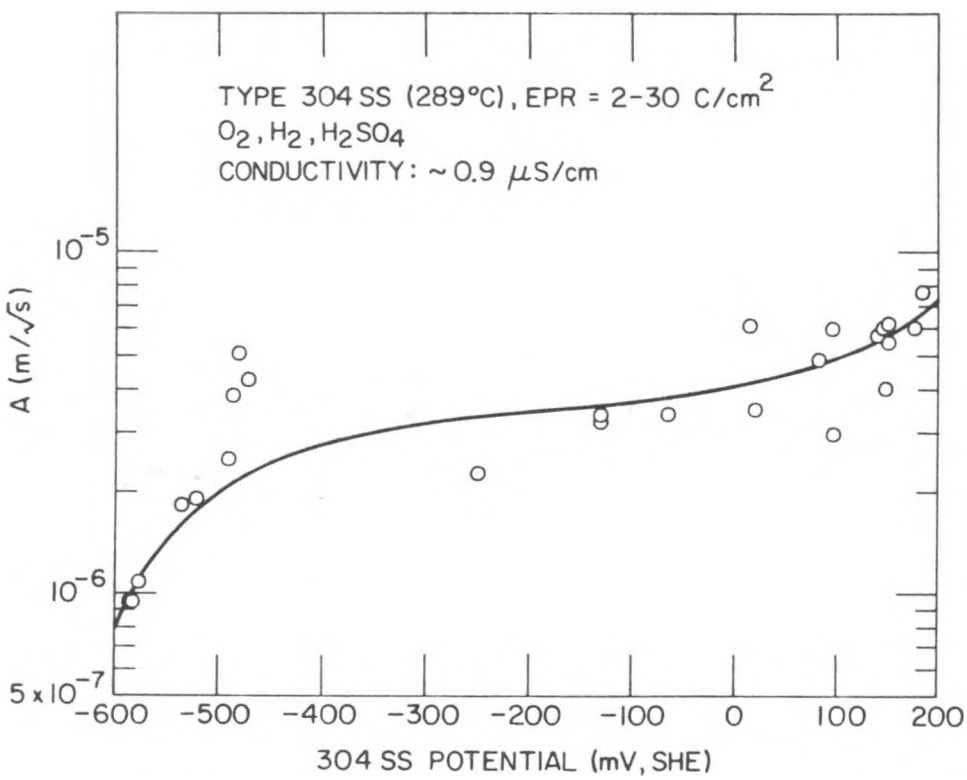

Fig. 21. Relationship between A and Open-Circuit Corrosion Potential in Water Containing 0.1 ppm Sulfate.

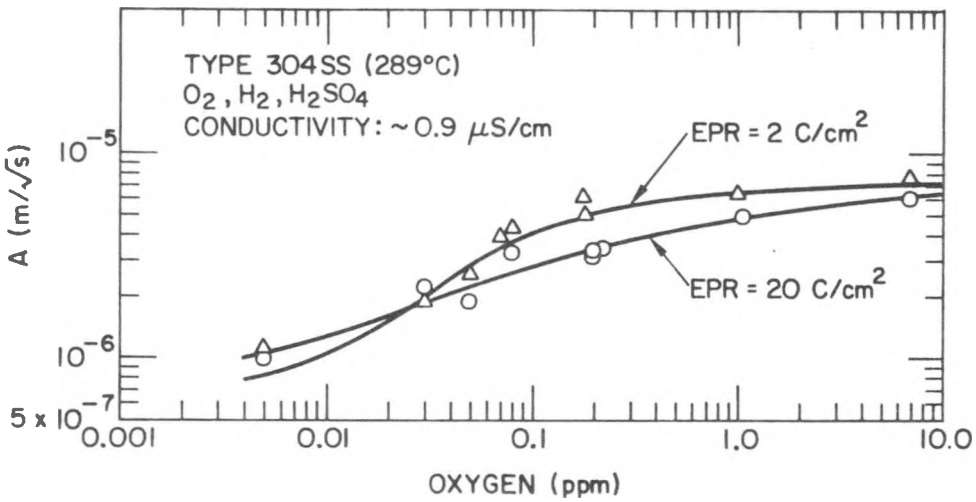

Fig. 22. Influence of Dissolved Oxygen in Water and DOS of Type 304 SS on A.

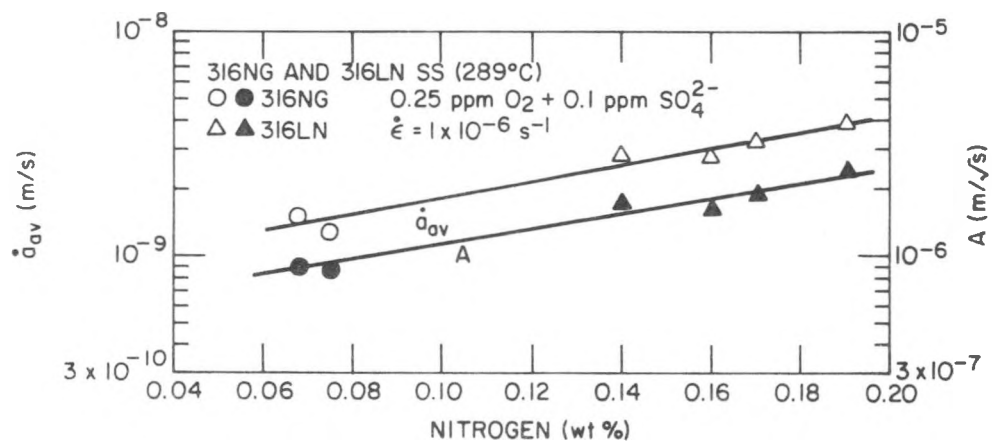

Fig. 23. Effect of Nitrogen Concentration on A and Average Crack Growth Rate for Types 316NG and 316LN SS.

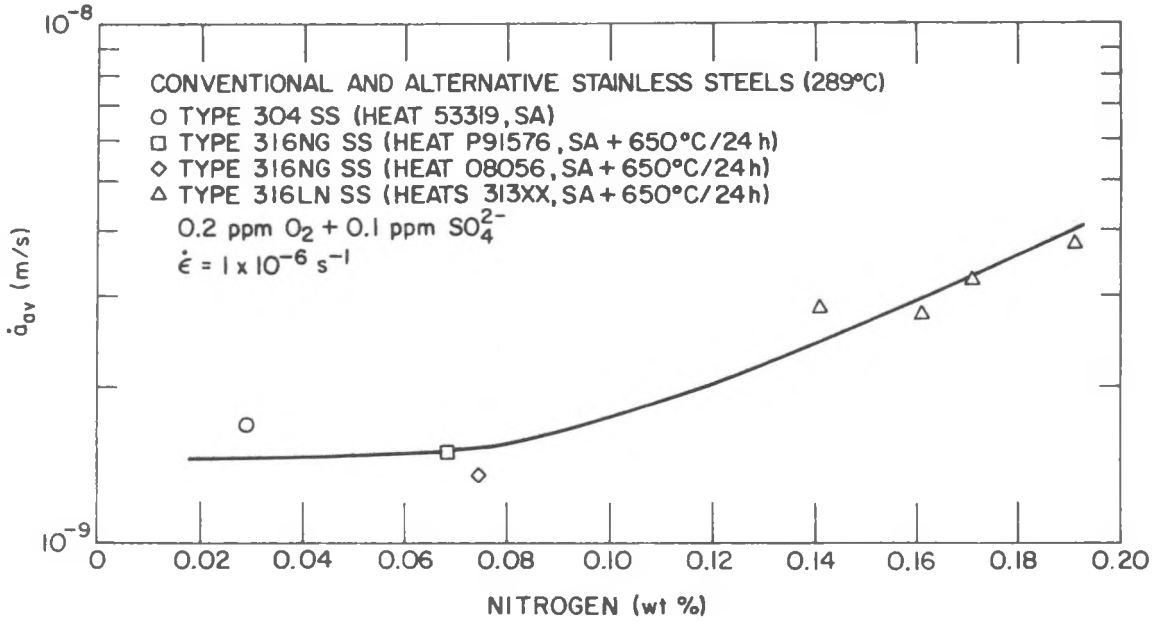

Fig. 24. Influence of Nitrogen Concentration on Average Transgranular Crack Growtih Rates for Austenitic Stainless Steels.

This result is consistent with extensive laboratory data obtained for Types 316NG, 316 and 304 SS in numerous environments, and recently the relationship has been applied to data from in-reactor experiments;[9] the agreement is again excellent as shown in Fig. 25. For tests at constant strain rate, power-law relationships are obtained between the SCC susceptibility parameters and the structure- and environment-dependent parameter A:

$$\dot{a}_{av} = (J_c/C\dot{\epsilon})^{-1/3} A^{4/3}, \tag{3}$$

$$a_f = (J_c/C\dot{\epsilon})^{1/3} A^{2/3}, \tag{4}$$

$$t_f = (J_c/C\dot{\epsilon})^{2/3} A^{-2/3}, \tag{5}$$

and

$$\epsilon_f = (J_c \dot{\epsilon}^{1/2}/C)^{2/3} A^{-2/3}. \tag{6}$$

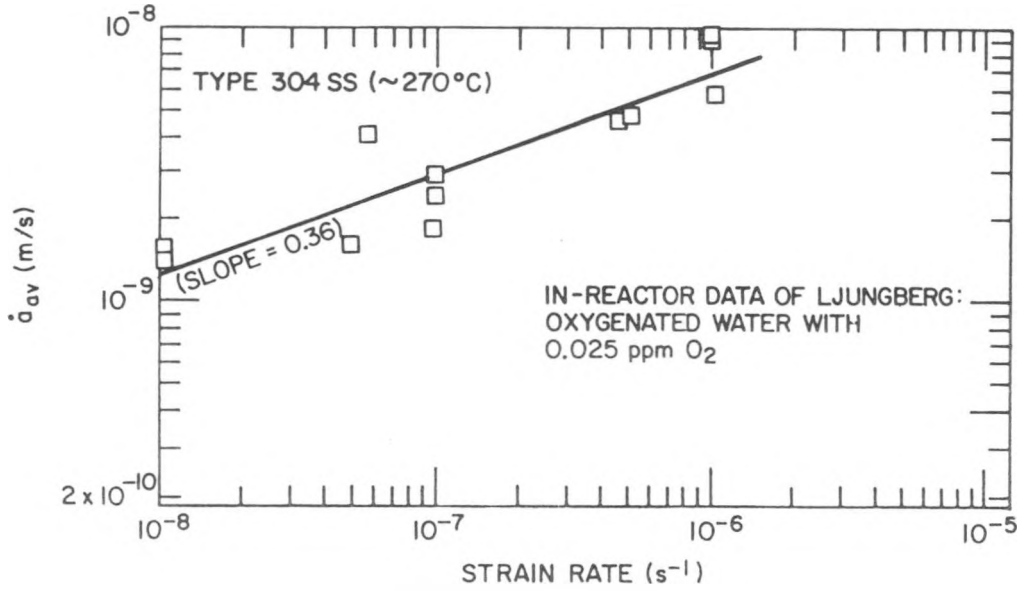

Fig. 25. Average Crack Growth Rate as a Function of Strain Rate for Type 304 SS. Data were obtained in the Ringhals-1 reactor in Sweden.[9]

The model expresses the crack growth rate constant A in terms of a_f and t_f, $A = a_f(t_f - t_o)^{-0.5}$ where it is assumed that the crack length at initiation is negligible compared to a_f and that crack initiation occurs at a strain of 1% so that $t_o = 0.01/\dot{\varepsilon}$. The relationship between $\dot{a}_{av}$ and A in high-purity water for Type 304 SS sensitized to EPR values of 2 and 20 C/cm^2 is shown in Fig. 26. The experimentaly determined slope is in good agreement with the value of 4/3 predicted by Eq. (3). The results in impurity environments show similar agreement with the model (Fig. 27). The variation of other SCC parameters such as a_f, t_f, and ε_f with A was also found to be consistent with the model, e.g., the dependence of a_f on A [Eq. (4)] is shown in Fig. 28.

The results in Fig. 29 show that the synergistic effects of impurities and the degree of sensitization can be accounted for by the variation of A as predicted by the model. In these tests, the impurity concentrations (viz., sulfate and chloride) were varied in water containing 0.25 and 8 ppm dissolved oxygen, and the experiments were conducted on material sensitized to 0, 11, and 24 C/cm^2. Similar agreement between the model

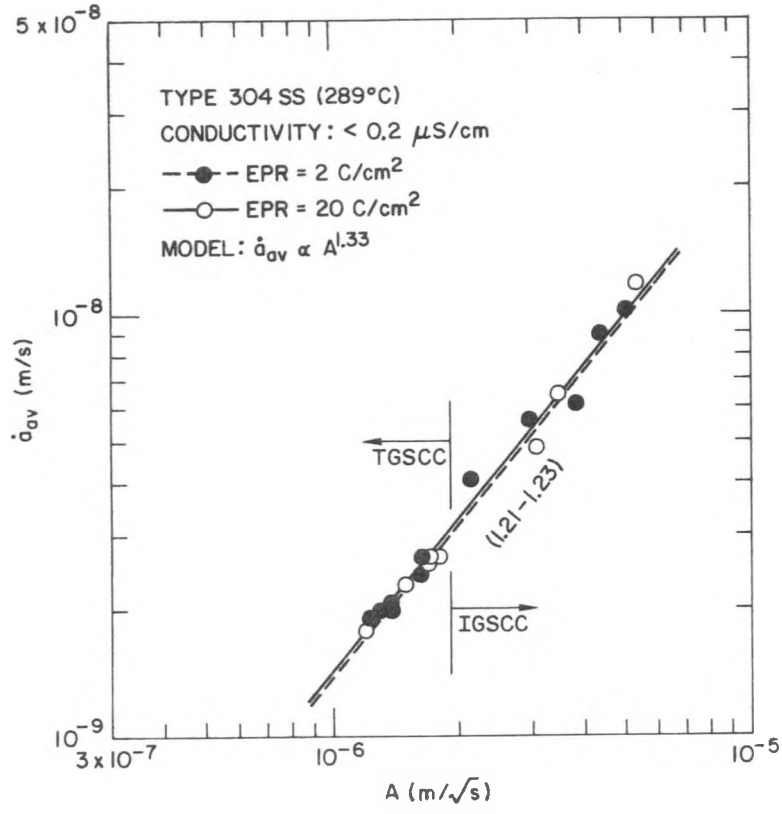

Fig. 26

Variation of Average Crack Growth Rate with the Model Crack Growth Parameter $[A = a_f(t_f - t_c)^{-0.5}]$ for Sensitized Type 304 SS in High-Purity Water Containing Different Concentrations of Dissolved Oxygen. Slopes are given in parentheses.

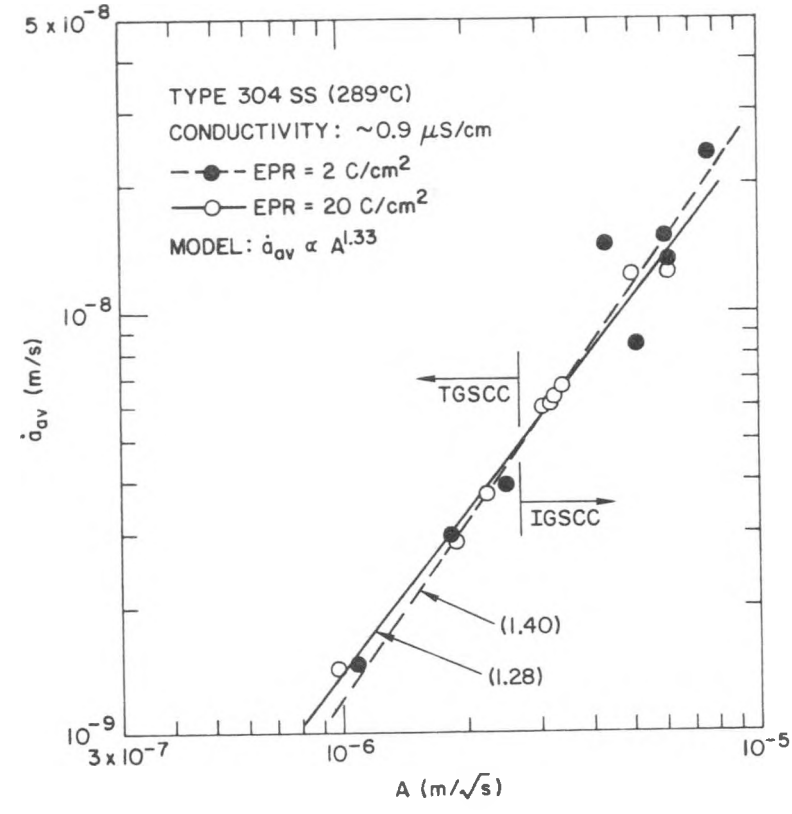

Fig. 27

Variation of Average Crack Growth Rate with the Model Crack Growth Parameter $[A = a_f(t_f - t_o)^{-0.5}]$ for Sensitized Type 304 SS in an Impurity Environment with 0.1 ppm Sulfate as H_2SO_4 and Different Concentrations of Dissolved Oxygen. Slopes are given in parentheses.

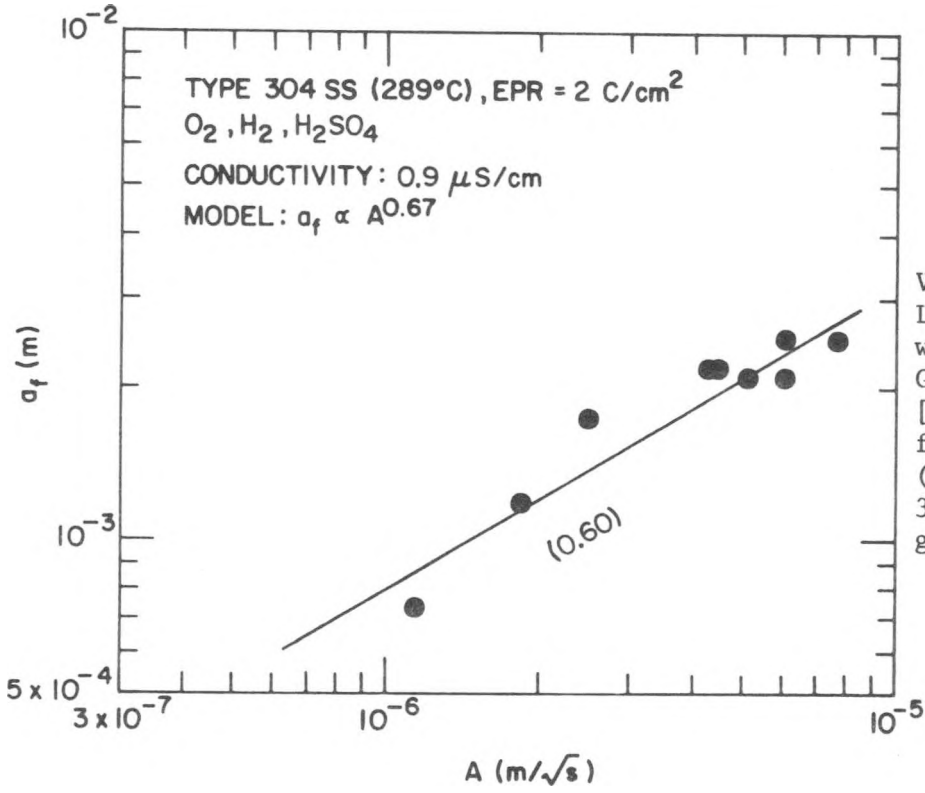

Fig. 28

Variation of Crack Length at Failure with the Model Crack Growth Parameter $[A = a_f(t_f - t_o)^{-0.5}]$ for Sensitized (EPR = 2 C/cm^2) Type 304 SS. The slope is given in parentheses.

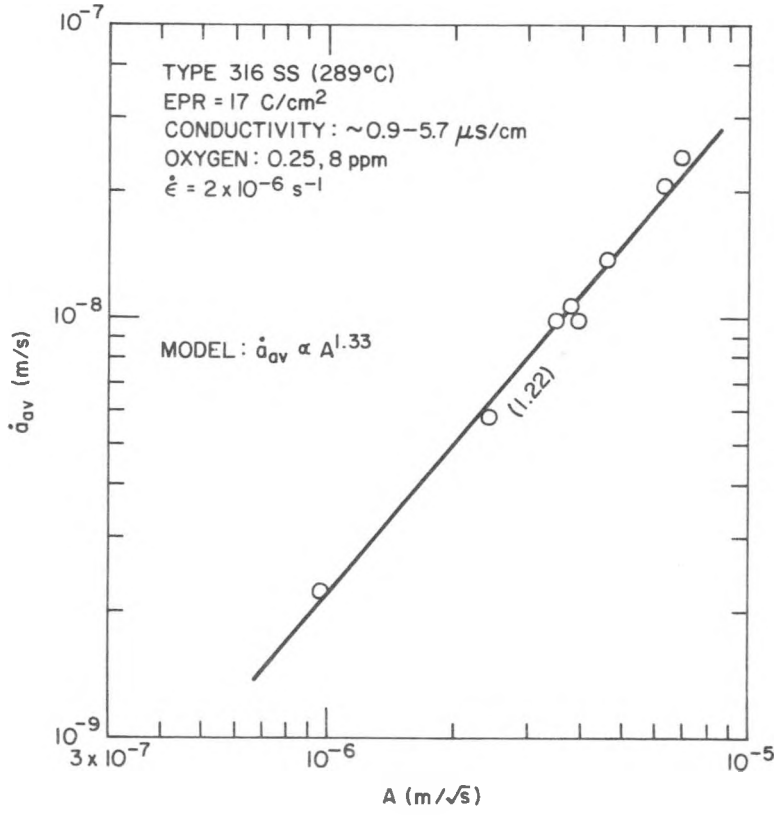

Fig. 29

Variation of Average Crack Growth Rate with the Model Crack Growth Parameter $[A = a_f(t_f - t_o)^{-0.5}]$ for Unsensitized and Sensitized Type 304 SS in Impurity Environments. The slope is given in parentheses.

predictions and experimental results for Type 316 SS sensitized to an EPR value of 17 C/cm^2 is shown in Fig. 30. Data in Fig. 31 show that variations in A also can correlate inherent differences in material resistance to crack growth for a number of alternative materials such as Types 316NG, 316LN, and 347NG SS. (In this plot, it is assumed that the fracture-characterizing parameter is the same for all the materials.) All the results in Fig. 31 were obtained in water containing 0.25 ppm oxygen and 0.1 ppm sulfate at a strain rate of 2×10^{-7} s^{-1} so that any differences can be attributed to the materials.

Currently, it is not possible to derive a relationship between A and corrosion potential, impurity level, or degree of sensitization based on fundamental considerations. However, empirical correlations derived from existing data (which are appropriate within the range of the experimental data) can be used to compare results obtained by different investigators.

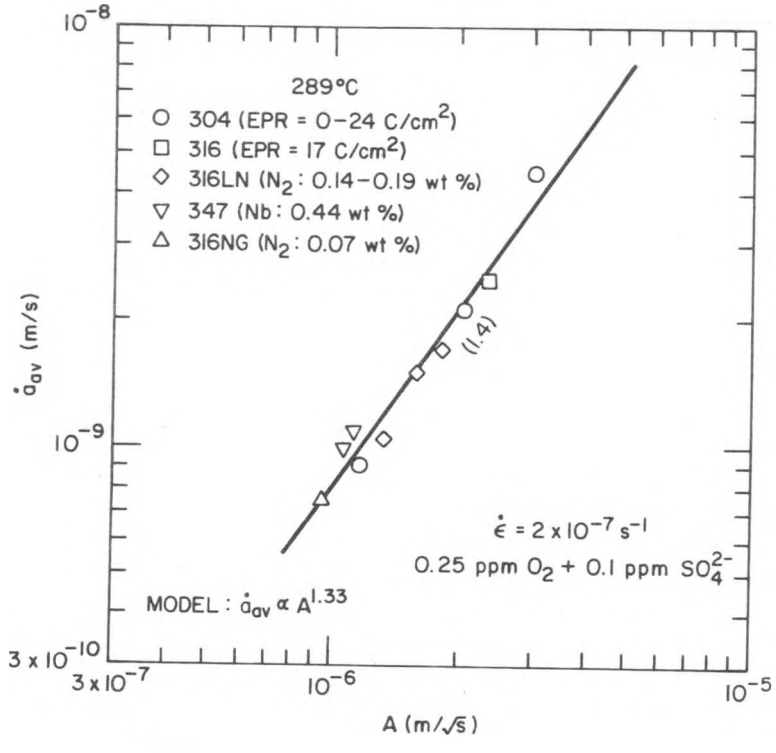

Fig. 30. Variation of Average Crack Growth Rate with the Model Crack Growth Parameter [$A = a_f(t_f - t_o)^{-0.5}$ for Sensitized Type 316 SS in Impurity Environments. The slope is given in parentheses.

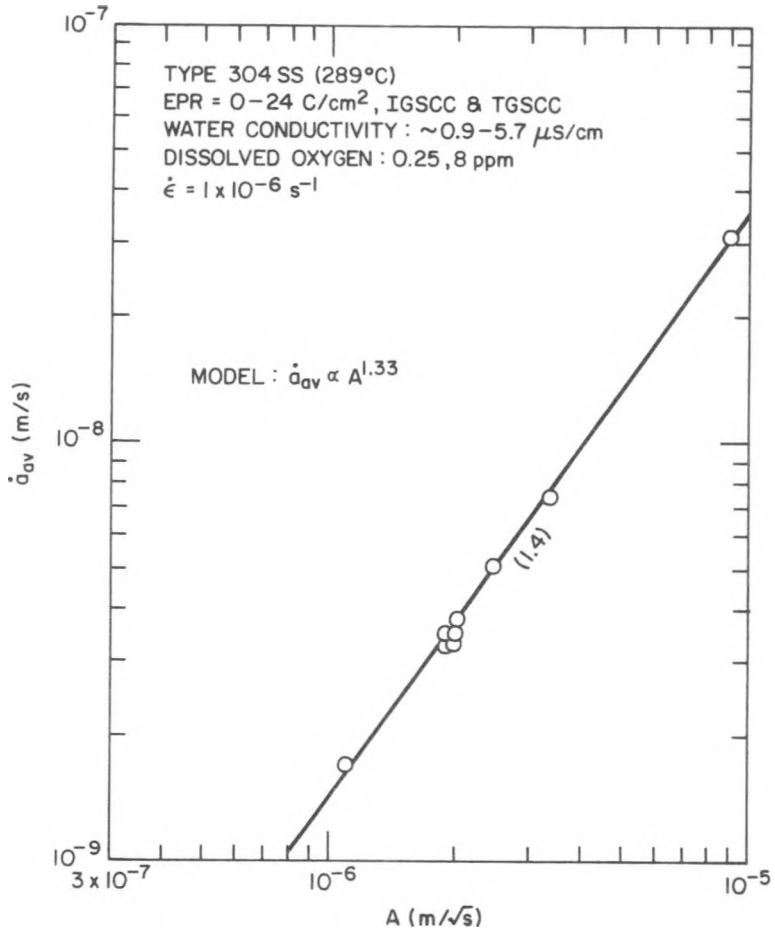

Fig. 31. Variation of Average Crack Growth Rate with the Model Crack Growth Parameter [$A = a_f(t_f - t_o)^{-0.5}$] for Several Austenitic Stainless Steels in Water Containing 0.25 ppm Dissolved Oxygen and 0.1 ppm Sulfate. The slope is given in parentheses.

For example, we have used the model and analyses to compare the results pertaining to the effects of dissolved oxygen or open-circuit corrosion potential on the SCC of Type 304 SS obtained at ANL[10] with those obtained by Indig and Weber[11] at the Dresden-2 reactor. This comparison is shown in Table 11. Although the excellent agreement between the predictions based on ANL results and the in-reactor data may be fortuitous, the consistency regarding the benefits of reducing the dissolved-oxygen concentration in laboratory tests and in-reactor experiments is encouraging. Future modeling efforts will focus upon a better understanding of SCC results obtained by means of different testing techniques.

TABLE 11. CERT Test Results in High-Purity Water at ∿274°C and a Strain Rate of ∿3.5 x 10^{-7} s^{-1}

Dissolved O_2, ppm	t_f, h Exp (Pred)[a]	ε_f, % Exp (Pred)[a]
Laboratory Results (Type 304 SS, Welded + LTS)		
0.18	224.0 (225)	26.8 (26.6)
0.09	293.5 (280)	36.3 (33.2)
In-Reactor Results[b] (Type 304 SS, SA + 621°C/24 h)		
0.2	108.0 (112.0)	12.1 (14.8)
0.04	143.0 (139.5)	20.3 (18.4)

[a]Based on ANL model.
[b]Reference 11.

C. Evaluation of Environmental Corrective Actions (W. E. Ruther, W. K. Soppet, T. F. Kassner, and W. J. Shack)

1. Introduction

The objective of this subtask is to evaluate the potential effectiveness of proposed actions to solve or mitigate the problem of IGSCC in BWR piping and safe ends through modifications of the water chemistry. In this regard, the synergistic effects of dissolved oxygen (produced by radiolytic decomposition of the water) and impurities (e.g., oxyacids from decomposition of ion exchange resins during periodic intrusions into the primary system) on the IGSCC susceptibility and crack growth properties of sensitized Type 304 SS have been evaluated. The potential benefits associated with small additions of hydrogen to the coolant were also evaluated under conditions in which ionic impurities were also present at low concentrations in the high-temperature water.

The results of this work indicate that SCC of the steel appears to be controlled by the rate of cathodic reduction of dissolved oxygen and/or oxyanion impurity species in the high-temperature water.[12,13] To explore this premise further, CERT experiments were performed in 289°C water containing sulfate and $Na_2B_4O_7$ at a low dissolved-oxygen concentration.[14] The addition of $Na_2B_4O_7$ to the feedwater provides an anion that is relatively innocuous from the standpoint of SCC, and which could adsorb on the oxide surface and conceivably compete for sites available for sulfate reduction. $Na_2B_4O_7$ also increases the pH of the feedwater and could decrease the rate of cathodic reduction of sulfate by the law of mass action, since the reactions are favored in acidic solutions. The results in water containing 10 ppm sulfate and $Na_2B_4O_7$ indicated that the SCC susceptibility decreases markedly when the borate/sulfate mole ratio was greater than 1. However, several ancillary experiments revealed that the increase in pH may have had a larger effect on mitigating SCC than the actual borate ion concentration of the feedwater.

During this reporting period, the influence of $Na_2B_4O_7$ on the SCC susceptibility of the steel was investigated in CERT experiments at 289°C in water containing 0.2 ppm dissolved oxygen. The effect of strain rate on SCC

of two heats of the steel was also investigated over the range of 2×10^{-8} to 1×10^{-4} s^{-1} in water containing different dissolved-oxygen and impurity levels. Initial results have been obtained from a long-term crack growth experiment at 289°C on a fracture-mechanics-type specimen fabricated from a weld overlay that was applied to a 10-in.-diameter schedule 140 pipe.

2. Technical Progress

a. Effect of $Na_2B_4O_7$ and pH on the SCC Susceptibility of Sensitized Type 304 SS in 289°C Water Containing 0.2 ppm Dissolved Oxygen

The premise that the rate of stress corrosion crack growth in sensitized Type 304 SS is controlled by the rate of cathodic reduction of species such as dissolved oxygen and/or various oxyanions present in high-temperature water suggests several environmental modifications to mitigate the problem. For example, if the rate of reduction of dissolved oxygen or the oxyanions (e.g., sulfate) depends on the kinetics of the adsorption/desorption process involving O_2/OH^- or SO_4^{2-}/SO_3^{2-} at the bulk-water/corrosion-product interface, ions that are innocuous from the standpoint of SCC (e.g., BO_3^{3-} or $B_4O_7^{2-}$) and which occupy surface sites available for electron transfer and reduction of O_2 or SO_4^{2-} could decrease the cathodic current (i_c), which couples with the anodic current (i_a) from the dissolution reaction at the crack tip. Another alternative involves increasing the pH of the bulk water, since all of the cathodic reduction reactions are more favorable in acidic or near-neutral solutions. The extent to which these factors influence SCC susceptibility of sensitized Type 304 SS was explored in a series of CERT experiments in 289°C water containing sulfate at a low dissolved-oxygen concentration (<0.005 ppm).[14] An analogous set of experiments was performed in water containing 0.2 ppm dissolved oxygen and 0.1 to 50 ppm $B_4O_7^{2-}$ as $Na_2B_4O_7$. To determine the role of pH in SCC in the oxygenated environment, two CERT tests were performed in water containing dissolved oxygen and 550 ppm H_3BO_3, in which the pH was adjusted with LiOH. Boric acid and sodium pentaborate are common chemicals that are used for continuous reactivity control in the primary coolant of PWRs and for a standby-liquid-control system in BWRs. In BWRs, the sodium pentaborate solution can be used to provide protection against an anticipated-transient-without-scram event.

The feedwater chemistries, CERT parameters, and electrochemical potential values for the steel and a platinum electrode are summarized in Table 12. The time to failure and the crack growth rate results are plotted as a function of the borate concentration in Fig. 32. In Fig. 32, the logarithmic concentration scale is broken at the extreme left to include a result obtained in high-purity water with 0.2 ppm dissolved oxygen (no borate). The data obtained in water containing 550 ppm H_3BO_3 are also included in the figure. The results indicate that borate does not have any beneficial effect on mitigating SCC of lightly sensitized Type 304 SS in water containing dissolved oxygen. Within the variability of the data in Fig. 32b, the intergranular crack growth rate in water containing 0.2 ppm oxygen and >0.5 ppm $B_4O_7^{2-}$ is approximately 7 x 10^{-9} m•s^{-1}. Furthermore, identical results (1 x 10^{-8} m•s^{-1}) were obtained in the two experiments with 550 ppm H_3BO_3, in which the pH was adjusted with 4 and 30 ppm LiOH. The concentration of the two species in the former environment simulates the water chemistry of the primary coolant in a typical PWR near the end of the fuel cycle, except for the relatively high dissolved-oxygen concentration (i.e., 0.2 vs. 0.005 ppm). In contrast to the results obtained in borate/sulfate solutions at a low dissolved-oxygen concentration (0.005 ppm),[14] in which the transgranular crack growth rate was ~2.5 x 10^{-9} m•s^{-1}, it is evident that a pH of >8.4 also has no beneficial effect on SCC of the steel in oxygenated water. Thus, it appears that neither the possible occupation of surface sites by the borate ions nor the concomitant increase in pH of the bulk water containing $Na_2B_4O_7$ has any effect on the rate of reduction of dissolved oxygen, which is the mostly likely partial process that couples with anodic dissolution at the crack tip in a slip-dissolution mechanism[15,16] for crack growth in the sensitized steel.

The dependence of the electrochemical potentials of the steel and platinum on the borate concentration in water containing 0.2 ppm dissolved oxygen is shown in Fig. 33. Although both the open-circuit corrosion potential of the steel and the redox potential of the platinum electrode decrease as the borate concentration in the oxygenated water increases, the values in Fig. 33 are considerably higher than those in borate/sulfate solutions with a low dissolved-oxygen concentration [i.e., -600 to -800 mV(SHE)], whereupon the crack growth rate decreased markedly and a transition from intergranular to transgranular fracture occurred.[14]

TABLE 12. Influence of $Na_2B_4O_7$ on the SCC Susceptibility of Sensitized Type 304 SS Specimens[a] in 289°C Water Containing ~0.2 ppm Dissolved Oxygen

	Feedwater Chemistry					CERT Parameters						Potentials	
Test No.	$B_4O_7^{2-}$, ppm	O_2, ppm	Molar Ratio	Cond., at 25°C, µS/cm	pH at 25°C	t_f, h	σ_{max}, MPa	Total Elong., %	Reduction in Area, %	Fracture Morphology[b]	SCC Growth Rate,[c] $m \cdot s^{-1}$	Type 304 SS, mV(SHE)	Pt, mV(SHE)
A2	0	0.24	0	0.14	6.12	166	493	60	66	0.80D, 0.20T	4.0×10^{-9}	44	60
A51	0.1	0.26	0.08	0.21	6.40	142	523	51	68	0.88D, 0.12T	2.8×10^{-9}	5	-77
A136	0.5	0.22	0.5	1.1	8.34	65	418	23	29	0.45D, $0.55G_3$	6.0×10^{-9}	44	155
A132	1.0	0.22	0.9	2.1	8.69	51	377	18	23	0.33D, $0.67G_3$	1.6×10^{-8}	-84	53
A135	5.0	0.21	4.9	8.5	9.06	105	500	38	53	0.51D, $0.49G_3$	7.9×10^{-9}	-70	11
A133	10.0	0.22	9.0	15.8	9.13	103	502	37	48	0.68D, $0.32G_3$	4.8×10^{-9}	-163	-56
A134	50.0	0.24	42.9	66.0	9.23	84	440	30	41	0.50D, $0.50G_3$	6.4×10^{-9}	-194	-59
A138	(550)[d]	0.23	1300	10.9	7.51	79	439	29	50	0.49D, $0.51G_3$	1.0×10^{-8}	-42	33
A137	(550)[e]	0.22	1360	93.0	8.42	80	453	29	32	0.50D, $0.50G_3$	1.0×10^{-8}	-159	-70

[a]Lightly sensitized (EPR = 2 C/cm^2) specimens (Heat No. 30956) were exposed to the environments for ~20 h before straining at a rate of of 1×10^{-6} s^{-1}.

[b]Ductile (D), transgranular (T), granulated (G), and intergranular (I), in terms of the fraction of the cross-sectional area. Characterization of the fracture surface morphologies is in accordance with the illustrations and definitions in "Transgranular, Granulated, and Intergranular Stress Corrosion Cracking in AISI 304 SS," by H. D. Solomon, Corrosion 40(9), 493-506 (1984).

[c]SCC growth rates are based on measurement of the depth of the longest crack in an enlarged micrograph of the fracture surface and the time period from the onset of yield to the point of maximum load on the tensile curve.

[d,e]Concentration of BO_3^{3-} added as H_3BO_3 and pH adjusted with 4 and 30 ppm LiOH, respectively.

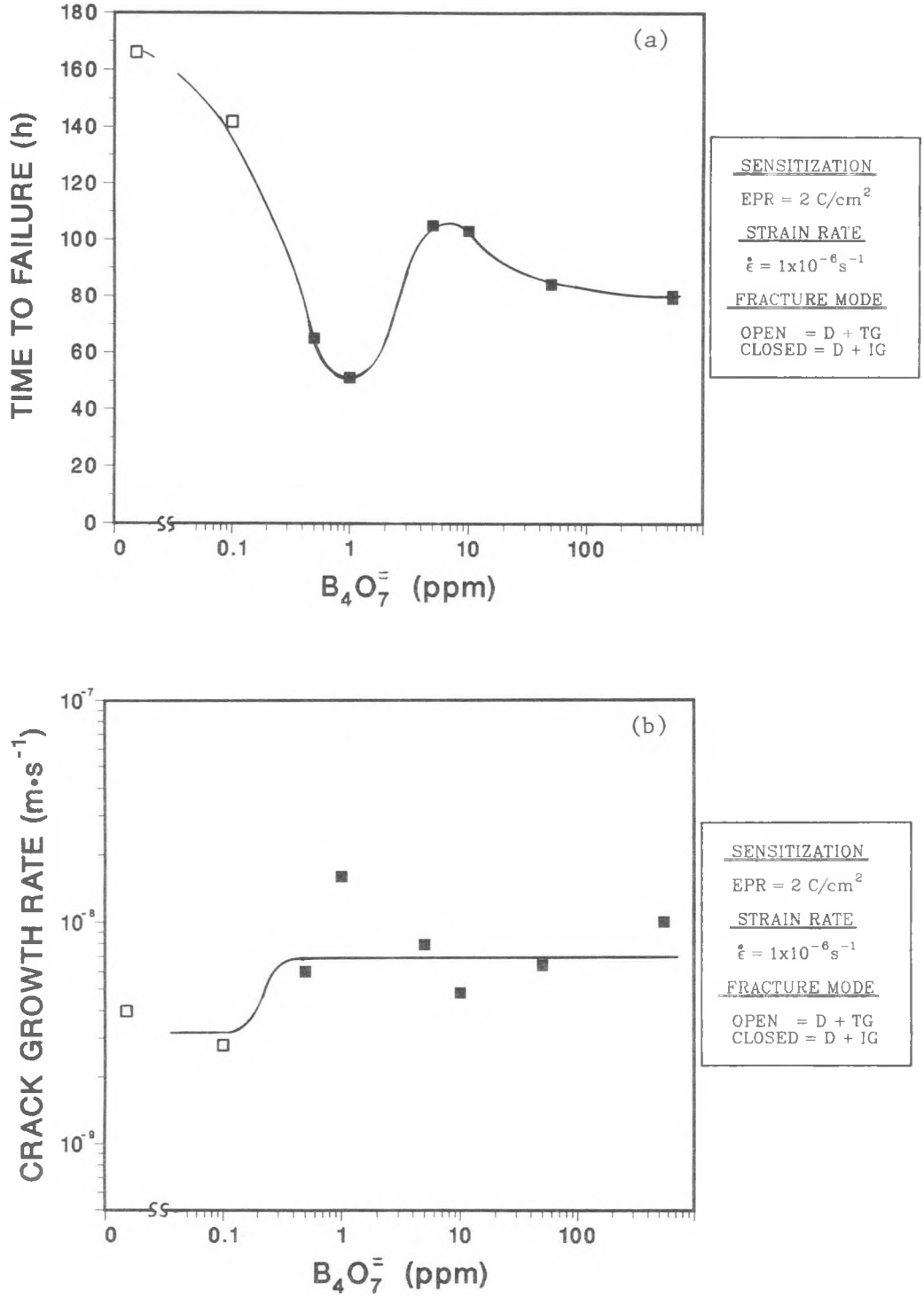

Fig. 32. (a) Time to Failure and (b) Crack Growth Rate for Lightly Sensitized (EPR = 2 C/cm^2) Type 304 SS CERT Specimens as a Function of Borate Concentration in 289°C Water Containing 0.2 ppm Dissolved Oxygen. Open and closed symbols denote ductile plus transgranular and ductile plus intergranular fracture morphologies, respectively.

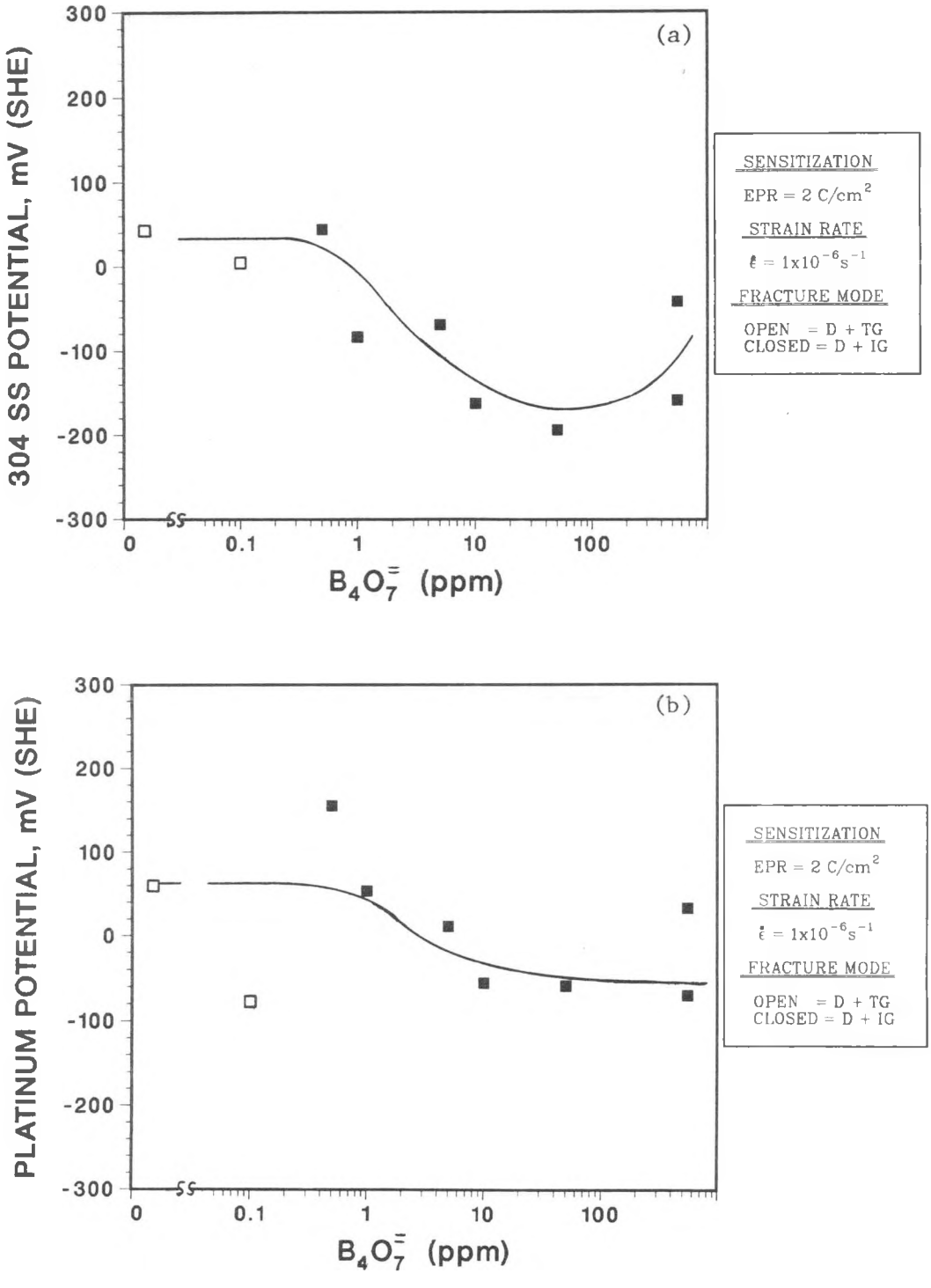

Fig. 33. Electrochemical Potential of (a) Type 304 SS and (b) Platinum as a Function of the Borate Concentration in 289°C Water Containing 0.2 ppm Dissolved Oxygen. Open and closed symbols denote ductile plus transgranular and ductile plus intergranular fracture morphologies, respectively.

The CERT tests on sensitized Type 304 SS in solutions containing boric acid and sodium tetraborate at 289°C reveal that the SCC behavior is primarily controlled by the dissolved-oxygen concentration of the water. In low-oxygen, H_3BO_3 environments, CERT experiments at a strain rate of 1×10^{-6} s^{-1} have shown that IGSCC does not occur and that the transgranular crack growth rate of the steel is quite low (i.e., $\sim 3 \times 10^{-9}$ $m \cdot s^{-1}$).[12,13] Other work[17] has shown that boric acid has almost no effect on IGSCC of sensitized Type 304 SS in CERT experiments in oxygenated water (2 and 8 ppm). Consequently, only in low-oxygen environments that contain deleterious impurities, such as sulfate, could IGSCC of sensitized Type 304 SS be mitigated by sodium tetra- or pentaborate additions (pH >8.4). No benefit would be derived by similar additions to oxygenated, high-temperature water.

b. Effect of Strain Rate on SCC Susceptibility of Sensitized Type 304 SS in 289°C Water with Different Dissolved-Oxygen and Impurity Concentrations

In the present program, the effect of strain rate in CERT experiments on intergranular- and transgranular-stress-corrosion cracking of Types 316 and 316NG SS, respectively, has been studied extensively in 289°C water containing dissolved oxygen and sulfate or chloride impurities.[1,18,19] A phenomenological model was also developed[1,7,19-21] that quantitatively describes relationships among the applied strain rate ($\dot{\varepsilon}$) and SCC parameters such as the time and strain to failure (t_f and ε_f), the crack length at failure (a_f), and the average crack growth rate ($\dot{a}_{av}$). In CERT tests carried to failure, the model predicts a power law dependence on the applied strain rate, viz., $t_f \sim \dot{\varepsilon}^{-2/3}$, $\varepsilon_f \sim \dot{\varepsilon}^{1/3}$, $a_f \sim \dot{\varepsilon}^{-1/3}$, and $\dot{a}_{av} \sim \dot{\varepsilon}^{1/3}$ [see Eqs. (3-6)]. In the case of Types 316 and 316NG SS, the CERT parameters follow these relationships over a fairly wide range of strain rate (e.g., 10^{-7} to 10^{-5} s^{-1}).[18-21] Such a relationship is expected to hold only for a range of strain rates between a lower and an upper threshold value. Below the lower threshold, the surface oxide film remains protective because the rupture rate is very low. Above the upper threshold value, the rate of crack growth is limited by the bare metal dissolution rate, and mechanical fracture predominates.[22]

The influence of strain rate on the SCC susceptibility of two heats of Type 304 SS in the lightly sensitized condition was investigated under different water chemistry conditions at 289°C. The feedwater chemistries, CERT parameters, and electrochemical potentials of the steel and platinum are given in Table 13. Strain rates between 10^{-4} and 10^{-8} s^{-1} were investigated. The dependence of the time to failure and the crack growth rate on strain rate for the steels in the two environments (i.e., 0.15 ppm O_2 plus 0.3 ppm SO_4^{2-} as H_2SO_4, and 0.005 ppm O_2 plus 5 ppm ClO_4^- as $HClO_4$) is shown in Fig. 34.

Over an intermediate range of strain rates, the log-log plots of t_f and $\dot{a}_{av}$ as a function of $\dot{\epsilon}$ yield straight lines with slopes that are in reasonable agreement with the strain rate exponents given by the model.[18-21] The present results deviate from the straight-line behavior at both low and high strain rates. As the strain rate increases, the fraction of the cross-sectional area on the fracture surface of the specimens that exhibits intergranular crack propagation decreases to the extent that purely ductile failures occur at the highest strain rates (see Table 13). In this regime, the contribution of stress corrosion to the fracture process is minimal. At very low strain rates, the fracture mode is predominantly intergranular; however, the crack growth rate, in particular, deviates significantly from the straight-line (slope = 1/3) behavior. The existence of threshold values of the strain rate has been established for a number of material-environment systems.[23] The upper threshold strain rates in our tests ($\sim 10^{-4}$-10^{-5} s^{-1}) are consistent with values generally observed for sensitized stainless steels in reactor-like environments,[24] but lower threshold strain rates in these systems have been generally assumed to be very low (i.e., $<10^{-9}$ s^{-1}).[24] The results shown in Fig. 34b suggest the existence of a lower threshold rate. However, since the fracture surface remains completely intergranular and there is no recovery in the ductility parameters such as the strain to failure or the reduction in area, the rapid decrease in the average crack growth rate at low strain rates is probably an artifact of the test specimen geometry. In the model,[18-21] crack growth is calculated based on the assumption of an edge crack in a semi-infinite space, i.e., there are no geometrical effects on crack growth. This gives a relation between the crack length and time at failure of the form:

TABLE 13. Influence of Strain Rate on the SCC Susceptibility of Sensitized Type 304 SS Specimens[a] in 289°C Water Containing Dissolved Oxygen and H_2SO_4 or $HClO_4$ at a Low Dissolved-Oxygen Concentration

			Feedwater Chemistry				CERT Parameters								Potentials	
Test No.	Heat No.	EPR,[b] C/cm^2	Oxygen, ppm	Sulfate/ Perchlorate, ppm	Cond., µS/cm	pH at 25°C	$\dot{\varepsilon}$, s^{-1}	t_f, h	σ_{max}, MPa	Total Elong., %	Reduction in Area, %	Fracture Morphology[c]	Crack Length, mm	SCC Growth Rate,[d] $m \cdot s^{-1}$	Type 304 SS, mV(SHE)	Pt, mV(SHE)
162	30956	2	0.16	0.3 (SO_4^{2-})	2.44	5.39	1×10^{-4}	1.5	501	55	74	1.00D	0	0	87	201
163			0.16		2.44	5.35	3×10^{-5}	4.7	496	51	64	0.87D, 0.13G_3	0.7	4.3×10^{-8}	66	-31
161			0.15		2.44	5.35	1×10^{-5}	11	467	39	48	0.60D, 0.40G_3	1.3	3.7×10^{-8}	93	205
160			0.16		2.44	5.37	1×10^{-6}	49	324	18	16	0.19D, 0.81G_3	2.0	1.6×10^{-8}	82	182
152			0.12		2.85	5.34	2×10^{-7}	142	246	10	12	0.10D, 0.90G_2	3.0	1.2×10^{-8}	54	-1
A139			0.14		2.65	5.35	1×10^{-7}	145	219	5.9	11	0.18D, 0.82I	3.0	8.2×10^{-9}	112	173
A141			0.15		2.70	5.30	5×10^{-8}	246	223	4.4	17	0.04D, 0.96I	3.1	5.1×10^{-9}	75	-99
A140			0.15		2.70	5.33	2×10^{-8}	498	220	3.6	13	0.05D, 0.95I	3.1	2.5×10^{-9}	68	174
168	9T2796	3	0.005	5.0 (ClO_4^-)	21.0	4.40	1×10^{-4}	1.4	449	50	71	1.00D	0	0	364	201
170			0.005		21.0	4.40	6×10^{-5}	2.3	449	50	68	1.00D	0	0	350	273
166			0.005[e]		23.0	4.35	3×10^{-5}	3.7	447	40	45	0.84D, 0.16G_3	0.7	5.6×10^{-8}	383	331
165			0.005[e]		23.0	4.35	1×10^{-5}	12.6	489	45	51	0.94D, 0.06G_2	0.8	1.9×10^{-8}	318	170
169			0.005		21.0	4.40	1×10^{-5}	13.9	461	50	67	1.00D	0	0	395	328
164			0.005[e]		22.5	4.34	1×10^{-6}	50	345	18	20	0.11D, 0.89G_2	2.8	1.9×10^{-8}	295	299
167			0.005[e]		23.0	4.36	2×10^{-7}	215	313	15	19	0.13D, 0.87G_3	2.8	4.5×10^{-9}	377	219
A142			0.005[e]		21.0	4.38	5×10^{-8}	634	230	11	6	0.09D, 0.91I	3.1	1.8×10^{-9}	162	226

[a] Specimens were exposed to the environment for ~20 h before straining at the different rates.
[b] Heat treatment at 700°C for 0.25 h was used to produce the EPR values for the two heats of steel. Specimens from Heat No. 30956 received an additional heat treatment for 24 h at 500°C.
[c] SCC growth rates are based on measurement of the depth of the longest crack in an enlarged micrograph of the fracture surface and the time period from the onset of yield to the point of maximum load on the tensile curve.
[d] Ductile (D), transgranular (T), granulated (G), and intergranular (I), in terms of the fraction of the cross-sectional area. Characterization of the fracture surface morphologies is in accordance with the illustrations and definitions in "Transgranular, Granulated, and Intergranular Stress Corrosion Cracking in AISI 304 SS," by H. D. Solomon, Corrosion 40(9), 493-506 (1984).
[e] Effluent dissolved oxygen concentration was 0.020-0.080 ppm by CHEMetrics measurements.

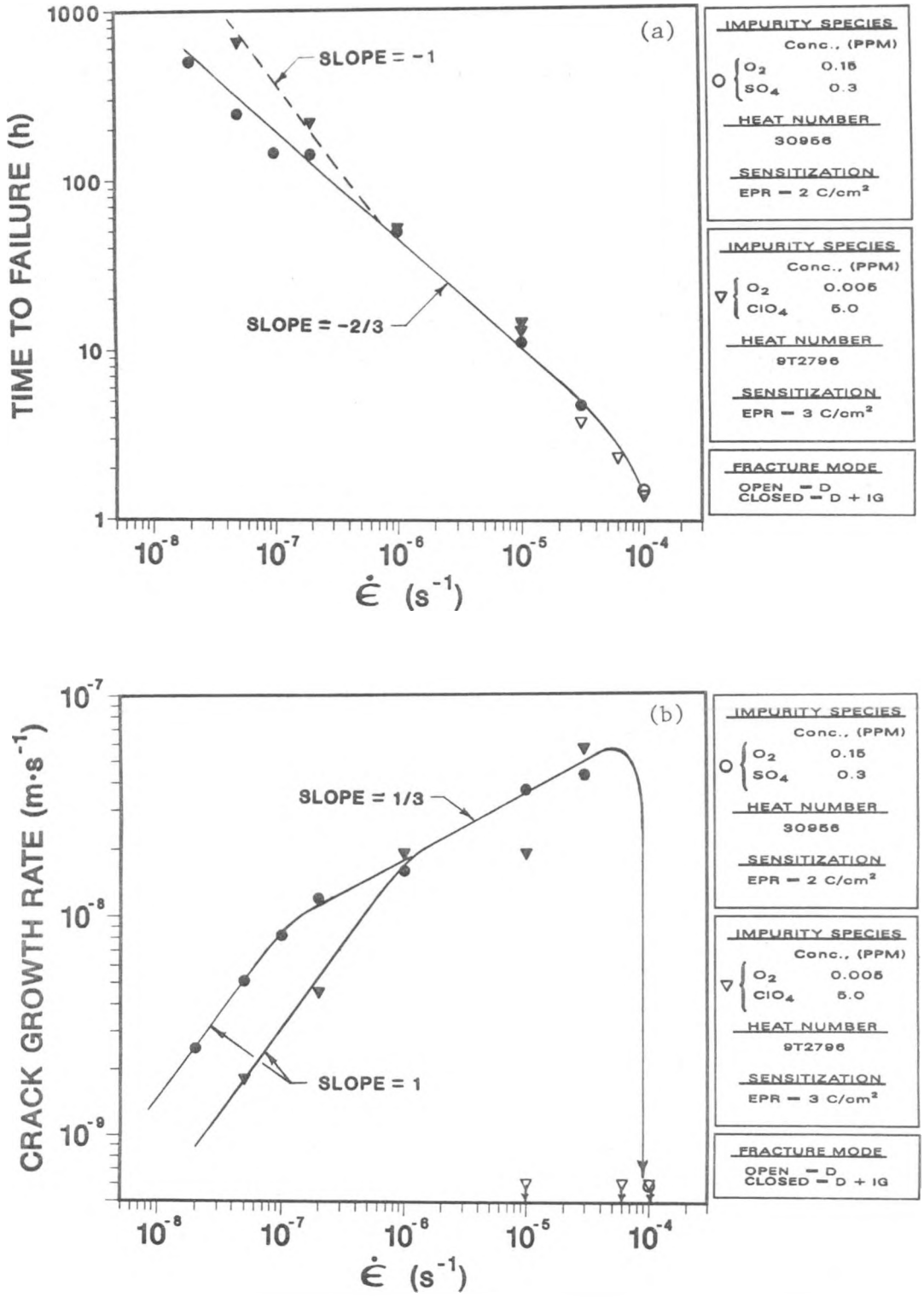

Fig. 34. Dependence of (a) Time to Failure and (b) Crack Growth Rate on Applied Strain Rate in CERT Experiments on Sensitized Type 304 Stainless Steels in 289°C Water with Different Dissolved-Oxygen and Impurity Concentrations. Open and closed symbols denote ductile and ductile plus intergranular fracture morphologies, respectively.

$$a_f = At_f^{1/2}, \tag{7}$$

where A is a constant which depends on the material and environment. This relation, along with the failure criterion

$$J_c = C\varepsilon_f a_f, \tag{8}$$

(where J_c is the value of the J-integral at failure and C is a constant which depends on the material and specimen geometry) can be used to determine the dependence of the parameters in the CERT test, such as the average crack velocity, on the nominal strain rate. For small specimens at low strain rates where almost the entire fracture surface undergoes stress corrosion with a small reduction in a cross-sectional area, the crack length at failure may be limited by the specimen geometry rather than by Eq. (7), i.e., at failure,

$$a_f = a_o, \tag{9}$$

where a_o is a characteristic crack length, viz., the radius for a cylindrical CERT specimen. If failure is determined by Eqs. (8) and (9), then the average crack velocity depends linearly on the nominal strain rate,

$$\dot{a}_{av} \sim \dot{\varepsilon}, \tag{10}$$

and a log-log plot of $\dot{a}_{av}$ as a function of $\dot{\varepsilon}$ gives a slope of 1. This behavior is consistent with the data shown in Fig. 34b and the appearance of the fracture surfaces.

Additional tests with different specimen geometries are needed to confirm that the threshold effects shown in Fig. 34 are an artifact of the test procedure. The existence of a true lower threshold strain rate has important implications for the extrapolation of crack growth rates obtained in the intermediate strain rate regime used for most laboratory tests to the lower strain rates that are characteristic of actual piping systems. However, it is important to recall that, although there is a fundamental relationship between the instantaneous crack growth rate and the crack tip strain rate, the

corresponding relationship between the average crack growth rate and the nominal strain rate may be dependent on the test procedure, and care should be exercised in the interpretation and extrapolation of such data.

c. Crack Growth in a Type 304 SS Weld Overlay Specimen under Cyclic Loading in Simulated BWR-Quality Water

To characterize the inherent crack growth resistance of the Type 308L weld metal used for weld overlay repairs, a long-term experiment is in progress on a fatigue precracked fracture-mechanics-type specimen fabricated from a 10-in.-diameter schedule 140 Type 304 SS pipe with a weld overlay applied by NUTECH Engineers and GAPCO Welding in accordance with their standard practice for overlay repairs. The 1TCT specimen was fabricated such that the crack will propagate through the original material and into the ER 308L SS overlay. The composition of the pipe and overlay material is given in Table 14. The base material was furnace sensitized at 600°C for 24 h, which produced an EPR value of 28 C/cm^2, before the overlay was applied. The ferrite content of the overlay was 12 ± 0.5%, as measured by a Ferrite Scope, Auto Test FE, Type FSP-1 probe.

The specimen was fatigue precracked in air at 289°C to a depth of ~6.6 mm at an R value of 0.2, a frequency of 10 Hz, and a stress intensity value of 20 $MPa \cdot m^{1/2}$. The feedwater chemistry, loading parameters, electrochemical potentials of Type 304 SS and platinum, and initial crack growth results in 289°C water are given in Table 15. The crack length as a function of time during loading at an R value of 0.95, a frequency of 8×10^{-2} Hz, and K_{max} = 28-37 $MPa \cdot m^{1/2}$ is plotted in Fig. 35. The nominal location of the interface between the outer surface of the pipe and the weld overlay in relation to the crack depth is indicated by the arrow in the figure. There is no change in slope at the interface between the base metal and the overlay, which indicates that the crack growth rates in the original sensitized material and the weld overlay are virtually the same (viz., ~7.9×10^{-11} $m \cdot s^{-1}$). This value is somewhat lower than those obtained with other heats of Type 304 SS used in this program under the same loading and environmental conditions (i.e., $3.3 \pm 1.4 \times 10^{-10}$ $m \cdot s^{-1}$).[25-27] Since there is some uncertainty in the location of the interface between the base metal and the weld overlay,

TABLE 14. Chemical Composition (wt. %) of the Type 304 SS/ER 308L SS Weld Overlay Specimen

Heat No.	Cr	Ni	Mn	Si	Mo	Cu	C	N	P	S	Fe
					Type 304 SS Pipe[a]						
5-751	17.86	9.65	1.77	0.42	0.22	0.23	0.065	0.105	0.020	0.005	Bal.
					ER 308L SS Overlay						
5-46850	19.87	10.23	1.70	0.33	0.22	0.10	0.015	0.050	0.018	0.007	Bal.

[a]The 10-in.-diameter schedule 140 pipe was furnace-sensitized at 600°C for 24 h, which produced an EPR value of 28 C/cm^2.

TABLE 15. Crack Growth Results for a Type 304 SS Weld Overlay Specimen[a] Under Simulated BWR Conditions[b]

Test Cond.	Test Time, h	Water Chemistry: Oxygen, ppm	Water Chemistry: Sulfate, ppm	Water Chemistry: Cond., µS/cm	Potentials: Type 304 SS, mV(SHE)	Potentials: Pt, mV(SHE)	K_{max}, $MPa \cdot m^{1/2}$	Growth Rate, $m \cdot s^{-1}$
1	4 700	0.2-0.3[c]	0.1	0.85	+130	+170	28.6	2.5×10^{-10}
2	700 1540	7.8-8.5			+185	+225	29.5	1.0×10^{-10}
3	1540 8090	0.2-0.3[c]			+130	+170	31.2	7.9×10^{-11}
4	8260[d] 9290	0.2-0.3[c]			+130	+170	33.4	~0
5	9290 9600	0.2-0.3[d]			+130	+170	36.8	e

[a]Compact tension specimen (1TCT) of Type 304 SS with a weld overlay.
[b]The load ratio and frequency of the positive sawtooth waveform were 0.95 and 8×10^{-2} Hz, respectively.
[c]Feedwater oxygen concentration at the 0.2-0.3 ppm level was approximately a factor of 2 higher to compensate for oxygen depletion by corrosion of the autoclave system.
[d]Accidental 10% momentary overload of the specimen at 8260 h.
[e]Experiment in progress.

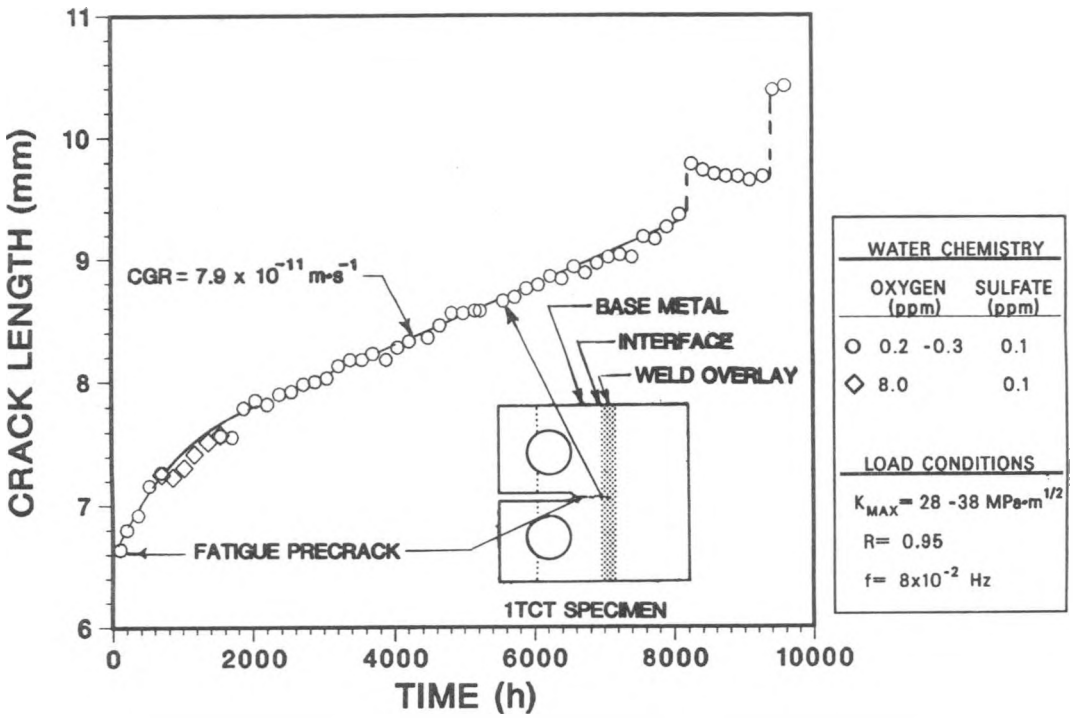

Fig. 35. Crack Length vs. Time for a 1TCT Specimen of Sensitized Type 304 SS with a ER 308L SS Weld Overlay in 289°C Water Containing 0.2 ppm Dissolved Oxygen and 0.1 ppm Sulfate as H_2SO_4. The specimen was subjected to low-frequency (8×10^{-2} Hz), high-R (0.95) loading at maximum stress intensities between 28 and 38 MPa$\cdot m^{1/2}$.

as well as in the measurement of the crack length by the compliance method, final confirmation that the crack has grown into the overlay will require metallographic examination of the specimen after completion of the test.

At 8260 h, the specimen was subjected to an accidental momentary overload of 10% of the maximum load, which blunted the crack and stopped its growth. The crack remained dormant for ~1000 h after the previous loading condition was restored. In an attempt to reinitiate crack growth in the material, the load was increased to the value that resulted during the overload. Preliminary measurements of crack growth by the compliance method indicate that crack growth has resumed at a rate commensurate with the higher stress intensity factor.

REFERENCES

1. W. J. Shack, "Measurement of Throughwall Residual Stresses in Large Diameter Piping Butt Weldments Using Strain Gage Techniques," in Residual Stress and Stress Relaxation, E. Kula and V. Weiss, eds., Plenum Press (1982), pp. 93-115.

2. E. F. Rybicki et al., Computational Residual Stress Analysis for Induction Heating of Welded BWR Pipes, EPRI NP-2662-LD, Electric Power Research Institute (December 1982).

3. P. S. Maiya and W. J. Shack, in Environmentally Assisted Cracking in Light Water Reactors: Annual Report, October 1983-September 1984, (June 1985), pp. 27-61.

4. J. M. Silcock, Effect of Nitrogen and Phosphorus on the Stress Corrosion Cracking of Austenitic Steels in $MgCl_2$ Solutions, Br. Corr. J. 17(4), 168-175 (1982).

5. D. L. Douglas, G. Thomas, and W. R. Roser, Ordering, Stacking Faults and Stress Corrosion Cracking in Austenitic Alloys, Corrosion 20(1), 15t-28t (1984).

6. P. S. Maiya and W. J. Shack, in Light-Water-Reactor Safety Materials Engineering Research Programs: Quarterly Progress Report, October-December 1984, NUREG/CR-3998 Vol. III, ANL-84-60 Vol. III (October 1985), pp. 14-23.

7. P. S. Maiya, "Prediction of Environmental and Strain Rate Effects on the Stress Corrosion Cracking of Austenitic Stainless Steels," in Predictive Capabilities in Environmentally Assisted Cracking, PVP-Vol. 99, R. Rungta, ed., Proc. Winter Ann. Mtg. of the American Society for Mechanical Engineers, New York (1985), pp. 39-54.

8. W. E. Ruther, W. K. Soppet, and T. F. Kassner, in Materials Science and Technology Division Light-Water-Reactor Safety Research Program: Quarterly Progress Report, October-December 1983, NUREG/CR-3689 Vol. IV, ANL-83-85 Vol. IV (August 1984), pp. 51-91.

9. Lars Ljungberg, in SCC Testing in BWR Environment, Report AA TR KM 83-285, SKI Project G.2.1/711/80, EPRI Project RP 1930-4 (1983).

10. P. S. Maiya, T. F. Kassner, and W. E. Ruther, "Analysis of the Effects of Corrosion Potential and Impurities on the Stress Corrosion Cracking of Type 304 Stainless Steel," in Environmental Degradation of Materials in Nuclear Power Systems-Water Reactors, Proc. 2nd Intl. Symposium, Monterey, CA, September 9-12, 1985, NACE (1986), pp. 77-83.

11. M. E. Indig and J. E. Weber, Effects of H_2 Additions on Stress Corrosion Cracking in a Boiling Water Reactor, Corrosion 41(1), 19-30 (1985).

12. W. E. Ruther, W. K. Soppet, and T. F. Kassner, in Light-Water-Reactor Safety Materials Engineering Research Programs: Quarterly Progress Report, January-March 1985, NUREG/CR-4490 Vol. I, ANL-85-75 Vol. I (March 1986), pp. 25-42.

13. W. E. Ruther, W. K. Soppet, and T. F. Kassner, in Environmentally Assisted Cracking in Light Water Reactors: Semiannual Report, April-September 1985, NUREG/CR-4667 Vol. I, ANL-86-31 Vol. I (June 1986), pp. 27-41.

14. Ibid., pp. 41-46.

15. F. P. Ford, "Stress Corrosion Cracking," in Corrosion Processes, R. N. Parkins, ed., Applied Science Publishers, New York (1982), pp. 271-309.

16. D. A. Vermilyea, in Proc. Intl. Conf. on Stress Corrosion Cracking and Hydrogen Embrittlement of Iron Base Alloys, R. W. Staehle, J. Hochmann, R. D. McCright, and J. E. Slater, eds., NACE, Houston (1983), p. 208.

17. K. Arioka, M. Hourai, S. Okamoto, and K. Onimura, The Effects of Boric Acid, Solution Temperature, and Sensitization on the SCC Behavior under Elevated Temperature Water, Corrosion 83, Anaheim, CA, April 18-22, 1983, Paper No. 135.

18. P. S. Maiya and W. J. Shack, in Environmentally Assisted Cracking in Light Water Reactors: Annual Report, October 1982-September 1983, NUREG/CR-3806 (June 1984), pp. 58-75.

19. P. S. Maiya and W. J. Shack, Stress Corrosion Cracking Susceptibility of AISI 316NG and 316 Stainless Steel in an Impurity Environment, Corrosion 41(11), 30-34 (1985).

20. P. S. Maiya and W. J. Shack, "Effects of Nominal and Crack-Tip Strain Rate on IGSCC Susceptibility in CERT Tests," in Embrittlement by the Localized Crack Environment (Proc. ASM Intl. Symp., Philadelphia, PA, October 4 and 5, 1983), AIME, Inc., New York, R. P. Gangloff, ed. (1984), pp. 199-209.

21. P. S. Maiya, "A Phenomenological Model for TGSCC in Type 316NG Stainless Steel," in Environmental Degradation of Materials in Nuclear Power Systems-Water Reactors (Proc. 2nd Intl. Symp., Monterey, CA, September 9-12, 1985), NACE (1986), pp. 12-17.

22. R. N. Parkins, "A Critical Evaluation of Current Environment-Sensitive Fracture Test Methods," in Environment-Sensitive Fracture: Evaluation and Comparison of Test Methods, ASTM STP 821, S. W. Dean, E. N. Pugh, and G. M. Ugiansky, eds., American Society for Testing and Materials, Philadelphia (1984), pp. 5-31.

23. G. M. Ugiansky and J. H. Payer, eds., Stress Corrosion Cracking - The Slow Strain Rate Technique, ASTM STP 665, American Society for Testing and Materials, Philadelphia (1979).

24. F. P. Ford, Mechanisms of Environmental Controlled Crack Propagation in Systems Peculiar to Power Generation, EPRI NP-1332-1, Electric Power Research Institute (August 1981).

25. W. E. Ruther, W. K. Soppet, and T. F. Kassner, in Light-Water-Reactor Safety Materials Engineering Research Programs: Quarterly Progress Report, January-March 1985, NUREG/CR-4490 Vol. I, ANL-85-75 Vol. I (March 1986), pp. 43-49.

26. W. E. Ruther, W. K. Soppet, and T. F. Kassner, in Environmentally Assisted Cracking in Light Water Reactors: Semiannual Report, April-September 1985, NUREG/CR-4667, Vol. I, ANL-86-31 Vol. 1 (June 1984), pp. 46-52.

27. J. Y. Park, W. E. Ruther, T. F. Kassner, and W. J. Shack, Stress Corrosion Crack Growth Rates in Type 304 Stainless Steel in Simulated BWR Environments, J. Eng. Mater. Technol. 108, 20-25 (1986).

Distribution for NUREG/CR-4667 Vol. II (ANL-86-37 Vol. II)

Internal:

O. K. Chopra
H. M. Chung
L. W. Deitrich
D. R. Diercks
F. Y. Fradin
B. R. T. Frost
D. M. Gruen
P. R. Huebotter
T. F. Kassner (10)
D. S. Kupperman
P. S. Maiya
V. A. Maroni
J. F. Marchaterre
K. Natesan
F. A. Nichols
J. Y. Park
W. E. Ruther
R. A. Scharping
W. J. Shack (5)
W. K. Soppet
E. M. Stefanski (2)
C. E. Till
R. A. Valentin
R. W. Weeks
H. Wiedersich
ANL Patent Dept.
ANL Contract File
ANL Libraries (2)
TIS Files (5)

External:

NRC, for distribution per R5 (350)
DOE-TIC (2)
Manager, Chicago Operations Office, DOE
R. Dalton, DOE-CH
Materials Science and Technology Division Review Committee:
C. B. Alcock, U. Toronto
A. Arrott, Simon Fraser U.
M. H. Cohen, Exxon Research and Engineering Co., Annandale, NJ
R. C. Dynes, AT&T Bell Labs., Murray Hill
A. G. Evans, U. California, Santa Barbara
E. Kay, IBM San Jose Research Lab.
M. B. Maple, U. California, San Diego
P. G. Shewmon, Ohio State U.
J. K. Tien, Columbia U.
J. W. Wilkins, Cornell U.
R. B. Adamson, General Electric Co., Vallecitos Nuclear Center, P. O. Box 460, Pleasanton, CA 94566
P. L. Andresen, General Electric Corporate Research and Development, Schenectady, NY 12301
G. A. Arlotto, Office of Nuclear Regulatory Research, USNRC, Washington
D. Atteridge, Battelle Pacific Northwest Lab., P. O. Box 999, Richland, WA 99352
W. H. Bamford, Structural Materials Engineering, Westinghouse Electric Corp., WNES, Box 355, Pittsburgh, PA 15230
W. Berry, Battelle-Columbus Labs., 505 King Ave., Columbus, OH 43201
C. Y. Cheng, Office of Nuclear Reactor Regulation, USNRC, Washington
W. J. Collins, Office of Inspection and Enforcement, USNRC, Washington
A. Cowan, Risley Nuclear Power Development Labs., U. K. Atomic Energy Authority, Risley, Warrington, WA3 6AT, England
G. Cragnolino, Brookhaven National Lab., Upton, NY 11973
R. M. Crawford, NUTECH Engineers, 225 N. Michigan Ave., Chicago, IL 60601
D. Cubicciotti, Electric Power Research Inst., P. O. Box 10412, Palo Alto, CA 94303
W. H. Cullen, Materials Engineering Assoc., Inc., 9700 B. George Palmer Highway, Lanham, MD 20706
J. C. Danko, AWTAC, New Topside Rd., Route 4, Box 90, Louisville, TN 37777
R. Duncan, Combustion Engineering, Inc., P. O. Box 500, Windsor, CT 06095

B. J. Elliot, Office of Nuclear Reactor Regulation, USNRC, Washington
M. Fox, Fox Enterprizes, 7490 Stanford Place, Cupertino, CA 95014
Y. S. Garud, S. Levy, Inc., 1901 S. Bascom Ave., Campbell, CA 95008
F. Garzarolli, KWU, Hammerbacherstr. 12+14, Postface:3220, 8520 Erlangen, West Germany
S. D. Harkness, Bettis Atomic Power Laboratory, P. O. Box 79, West Mifflin, PA 15122
D. O. Harris, 750 Welch Rd., Palo Alto, CA 94303
W. S. Hazelton, Office of Nuclear Reactor Regulation, USNRC, Washington
M. E. Indig, General Electric Co., P. O. Box 460, Pleasanton, CA 94566
H. S. Isaccs, Brookhaven National Laboratory, Upton, NY 11973
R. E. Johnson, Office of Nuclear Reactor Regulation, USNRC, Washington
R. H. Jones, Battelle Pacific Northwest Lab., P. O. Box 999, Richland, WA 99352
R. L. Jones, Electric Power Research Inst., P. O. Box 10412, Palo Alto, CA 94303
J. Kass, General Electric Co., 175 Curtner, San Jose, CA 95125
P. M. Lang, Office of Converter Reactor Deployment, USDOE, Washington 20545
L. Ljungberg, ASEA-ATOM, Box 53, S-721 04, Västerås, Sweden
C. D. Lundin, U. Tennessee, Knoxville, TN 37996-2200
D. D. Macdonald, SRI International, 333 Ravenswood Ave., Menlo Park, CA 94025
H. Metha, General Electric Co., 175 Curtner, San Jose, CA 95125
J. Muscara, Office of Nuclear Regulatory Research, USNRC, Washington
D. M. Norris, Electric Power Research Inst., P. O. Box 10412, Palo Alto, CA 94303
D. R. O'Boyle, Commonwealth Edison Co., P. O. Box 767, Chicago, IL 60690
R. A. Oriani, U. Minnesota, Minneapolis, MN 55455
S. Ranganath, General Electric Co., 175 Curtner, San Jose, CA 95125
J. T. A. Roberts, Battelle Pacific Northwest Lab., P. O. Box 999, Richland, WA 99352
E. J. Rowley, Commonwealth Edison Co., P. O. Box 767, Chicago, IL 60690
E. F. Rybicki, Dept. of Mechanical Engineering, U. Tulsa, Tulsa, OK 74110
C. Z. Serpan, Office of Nuclear Regulatory Research, USNRC, Washington
L. Shao, Office of Nuclear Regulatory Research, USNRC, Washington
R. D. Silver, Office of Nuclear Reactor Regulation, USNRC, Washington
S. Smialowska, Dept. of Metallurgical Engineering, Ohio State U., Columbus, OH 43210
L. J. Sobon, NUTECH Engineers, 6835 Via del Oro, San Jose, CA 95119
A. A. Solomon, School of Nuclear Engineering, Purdue U., West Lafayette, IN 47907
H. D. Solomon, General Electric, P. O. Box 43, Schenectady, NY 12301
D. M. Stevens, Lynchburg Research Center, Babcock & Wilcox Co., P. O. Box 239, Lynchburg, VA 24505
A. Taboada, Office of Nuclear Regulatory Research, USNRC, Washington
E. Venerus, Knolls Atomic Power Laboratory, P. O. Box 1072, Schenectady, NY 12301
J. R. Weeks, Brookhaven National Lab., Upton, NY 11973
K. R. Wichman, Office of Nuclear Reactor Regulation, USNRC, Washington
F. Witt, Office of Nuclear Reactor Regulation, USNRC, Washington
A. W. Zeuthen, Long Island Lighting Co., P. O. Box 618, Wading River, NY 11792